GALLIUM-DOPED ZINC OXIDE NANORODS FOR PHOTOCATALYTIC PERFORMANCE UNDER SOLAR IRRADIATION

SULAIMAN S.A. ALGHAFRI

FACULTY OF SCIENCE
UNIVERSITI MALAYA
KUALA LUMPUR

2022

GALLIUM-DOPED ZINC OXIDE NANORODS FOR PHOTOCATALYTIC PERFORMANCE UNDER SOLAR IRRADIATION

SULAIMAN S.A. ALGHAFRI

DISSERTATION SUBMITTED IN FULFILLMENT OF THE REQUIREMENTS FOR THE DEGREE OF MASTER OF SCIENCE

DEPARTMENT OF PHYSICS
FACULTY OF SCIENCE
UNIVERSITI MALAYA
KUALA LUMPUR

2022

UNIVERSITI MALAYA

ORIGINAL LITERARY WORK DECLARATION

Name of Candidate: **SULAIMAN S.A. ALGHAFRI**

Student ID: **S2024842/1**

Name of Degree: **MASTER OF SCIENCE**

Title of DISSERTATION:

GALLIUM-DOPED ZINC OXIDE NANORODS FOR PHOTOCATALYTIC PERFORMANCE UNDER SOLAR IRRADIATION

Field of Study: **PHYSICS**

I do solemnly and sincerely declare that:

(1) I am the sole author/writer of this Work;
(2) This Work is original;
(3) Any use of any work in which copyright exists was done by way of fair dealing and for permitted purposes and any excerpt or extract from, or reference to or reproduction of any copyrighted work has been disclosed expressly and sufficiently and the title of the Work and its authorship have been acknowledged in this Work;
(4) I do not have any actual knowledge nor do I ought reasonably to know that the making of this work constitutes an infringement of any copyrighted work;
(5) I hereby assign all and every right in the copyright to this Work to the University of Malaya ("UM"), who henceforth shall be owner of the copyright in this Work and that any reproduction or use in any form or by any means whatsoever is prohibited without the written consent of UM having been first had and obtained;
(6) I am fully aware that if in the course of making this work I have infringed any copyright, whether intentionally or otherwise, I may be subject to legal action or any other action as may be determined by UM.

Candidate's Signature Date: 8 Aug 2022

S Subscribed and solemnly declared

before, Witness's Signature

Date: 8 Aug 2022

Name:

Designation:

GALLIUM-DOPED ZINC OXIDE NANORODS FOR PHOTOCATALYTIC PERFORMANCE UNDER SOLAR IRRADIATION

ABSTRACT

In this thesis, a rapid microwave-assisted method has been used to synthesize pristine and gallium (Ga) doped ZnO nanorods on the glass substrates. With different percentages of the concentration of the gallium nitrate compound in the seeding and growth solutions, the samples were labeled to 0.5%, 1%, 3% and 5% Ga-doped ZnO nanorods. These samples were used to degrade artificial water pollutants by adding methylene blue dye in water and to track the percentage of analysis for each sample. Prepared samples were characterized by X-Ray Diffraction (XRD), Field Emission Scanning Electron Microscopy (FESEM), Energy Dispersive X-ray (EDX), Atomic Force Microscopy (AFM), UV-Vis spectroscopy, Photoluminescence (Shtepliuk) spectroscopy, Fourier Transform Infra-red (FTIR) spectroscopy, X-ray Photoelectron Spectroscopy (XPS) and methylene blue degradation photo-catalyst efficiency analysis. The degradation of methylene blue in the presence of a prepared sample has been followed systematically. The results showed that the diameter and length of the nanorods significantly change with Ga doping from 0% to 5% from 63.2 ± 0.2 to 85.2 ± 0.2 nm diameter and from 0.64 ± 0.01 to 2.08 ± 0.02 μm length. Comparably, the crystal orientation and surface oxidation states from mean crystallite grain size (D) and the FWHM values at the peak position are also Ga content dependent. The existence of Ga-O bonds in the ZnO lattice is evidenced by XRD, which confirms the effective Ga-doping of ZnO NRs. The 1% Ga doping sample showed significant enhancement in visible light absorption, effective change carrier separation, and rapid degradation rate (60 min) compared to the pristine sample.

Key words: Gallium, Doping, Nanorods, Photocatalysis, Pollution, Zinc Oxide.

GALLIUM-DOPED ZINC OXIDE NANORODS FOR PHOTOCATALYTIC PERFORMANCE UNDER SOLAR IRRADIATION

ABSTRAK

Dalam tesis ini, kaedah bantuan gelombang mikro pantas telah digunakan untuk mensintesis nanorod ZnO terdop tulen dan galium (Ga) pada substrat kaca. Dengan peratusan berbeza kepekatan sebatian galium nitrat dalam larutan pembenihan dan pertumbuhan, sampel telah dilabelkan dengan 0.5%, 1%, 3% dan 5% nanorod ZnO berdop Ga. Sampel ini digunakan untuk merendahkan bahan pencemar air tiruan dengan menambahkan pewarna biru metilena dalam air dan untuk mengesan peratusan analisis bagi setiap sampel. Sampel yang dicirikan dengan Pembezaan X-Ray (XRD), Mikroskopi Elektron Pengimbasan Pancaran Medan (FESEM), X-ray Penyerakan Tenaga (EDX), Mikroskopi Daya Atom (AFM), Spektroskopi UV-Vis, Spektroskopi Photoluminescence (Shtepliuk), Spektroskopi Fourier Transform Infra-merah (FTIR), Spektroskopi Fotoelektron X-ray (XPS) dan analisis kecekapan foto-mangkin degradasi biru metilena. Degradasi metilena biru dalam setiap sampel telah dikaji secara sistematik. Keputusan menunjukkan bahawa diameter dan panjang nanorod berubah dengan ketara dengan doping Ga daripada 0% kepada 5% iaitu 63.2 ± 0.2 kepada 85.2 ± 0.2 nm bagi diameter dan dari 0.64 ± 0.01 kepada 2.08 ± 0.02 μm bagi panjang nanorod. Orientasi hablur dan keadaan pengoksidaan permukaan daripada saiz butiran kristal (D) purata dan nilai FWHM pada kedudukan puncak juga bergantung kepada kandungan Ga. Kewujudan ikatan Ga-O dalam kekisi ZnO dibuktikan oleh XRD, yang mengesahkan keberkesanan Ga-doping ZnO NRs. Sampel doping Ga 1% menunjukkan peningkatan ketara dalam penyerapan cahaya yang boleh dilihat, pemisahan pembawa perubahan yang berkesan, dan kadar degradasi pesat (60 min) berbanding dengan sampel murni.

Kata kunci: Gallium, Doping, Nanorods, Photocatalysis, Pollution, Zinc Oxide.

ACKNOWLEDGEMENT

I extend my great thanks and gratitude to God Almighty, who enabled me to complete this humble work, which I would not have been able to complete without his success and facilitation.

I also thanks to my supervisors Assoc. Prof. Dr. Azzuliani Supangat and Dr. Mohammed Al-Abri who stood with me and facilitated obstacles and difficulties for me and helped me provide the appropriate research environment to complete my thesis. I also extend my thanks to my dear brothers Dr. Faisal and Dr. Bassem who, without them, would not have been able to complete this modest research.

I would like to acknowledge the financial support from the Ministry of Higher Education Malaysia under the Fundamental Research Grant Scheme (FP078-2018A) and Nanotechnology Research Center, Sultan Qaboos University, Oman. It is also extended to the Department of Physics, College of Science at Sultan Qaboos University, Oman.

I also extend my thank to my family who have supported me and inspired me to work hard.

TABLE OF CONTENTS

LIST OF FIGURES

LIST OF TABLES

LIST OF SYMBOLS AND ABBREVIATIONS

λ	:	Wavelength MB Methylene Blue
β	:	FWHM in radians
θ	:	Bragg's diffraction angle
δ	:	Dislocation density
α	:	Absorption coefficient
a,c	:	Lattice parameters
D	:	Mean crystallite size
d_{hkl}	:	Interplanar spacing
h,k,l	:	Miller indices denoting
AFM	:	Atomic Force Microscope
EDX	:	Energy-dispersive x-ray spectroscopy
E_g	:	Energy band gap
FTIR	:	Fourier-transform Infrared Spectroscopy
FWHM	:	Full Width Half Maximum
GZO	:	Ga-doped ZnO
NRs	:	Nanorods
RMS	:	Root-Mean-Square
UV-Vis	:	UV-Visible Spectroscopy
XRD	:	X-ray Diffraction

CHAPTER 1: INTRODUCTION

1.1 Background

1.1.1 Water Pollution

Water pollution is defined as the occurrence of changes in the nature, quality and properties of water. That make it unsuitable for use, as this occurs by adding foreign or polluting substances such as: chemicals, bacteria, or even in the form of thermal or radioactive energy to various aquatic ecosystems, whether groundwater or superficial such as lakes, streams, rivers, estuaries and oceans, and this in turn affects the performance of all different ecosystems (R. e. P. Schwarzenbach, 2012). In addition to the waste that floats on its surface, but in other cases no signs of contamination appear, indicating that it is saturated with chemicals that cannot be seen or smelled (Rajaram, 2008). The quality of water can be known and distinguished whether it is polluted by a set of water quality standards, such as chemical measures of water quality and measuring water quality chemically depending on the concentrations of chemicals in different water samples (Brix, 1995). Biometrics of water quality of the measurement depends biologically on the possibility of living organisms such as fish, insects, and other invertebrates in the water which can cause to the poor water quality and unusable (Rajaram, 2008).

From a health point of view, the pollution of consumed water is linked to the transmission of many serious diseases such as cholera, diarrhea, dysentery, hepatitis A, typhoid and polio. Some recent environmental studies published in some scientific journals indicate that diseases caused by polluted water are responsible for more than two million deaths and four billion cases of diarrhea worldwide annually. This in turn makes water pollution one of the main causes of death and disease (Gunkel, 2007). According to World Health Organization reports, in 2017,

more than 220 million people needed preventive treatments for schistosomiasis. This disease is an acute and chronic disease caused by parasitic worms that are found in contaminated water and transmitted through them to human bodies (Health, 2020). In addition to the direct and indirect effects on humans, polluted water may affect various economic and social aspects of human life. The World Bank issued a warning in 2019 that polluted water is slashing economic growth by up to a third in some countries. This was stated in a report published by the bank on its website (Health, 2020).

1.1.2 Polluted Water and Remediation Technology

There are many methods used to remediate water. All of these methods used differ in their quality and efficiency. One of the most prevalent methods is the distillation method, but one of its disadvantages is that most pollutants remain behind and require large amounts of energy and water (Schwarzenbach, 2012). One of the methods used is chemical transformation. This method requires excess reagents so that the product is of low quality and cannot be used well. Coagulation and flocculation are also used in water purification. This method is complex, less efficient and requires highly alkaline additions to achieve the optimum water pH. There is also a method of biological treatment in which microorganisms are used. Its disadvantages are that it is difficult to control, expensive and time-consuming (Kunduru, 2012).

Ultraviolet treatment is one of the methods used to purify water. This method is financially costly and disruptive due to water turbidity. The reverse osmosis method can also be used in this field, which removes minerals from the water. This method requires high effort and is ineffective in removing volatile organic matter, chemicals, chlorine, chloramine and drugs. Nanofiltration, ultrafiltration,

microfiltration and carbon filter, all of them are methods that use a narrow pore process to purify water that allows the passage of small particles and prevents the passage of large particles. These methods have a disadvantage in that they cannot remove many of the substances found in water, such as nitrates, fluoride, metals, sodium, volatile organics, and color (Xingjian, 2018).

Photocatalysis is one of the most promising modern methods used in water purification. In it, photocatalysts made of semiconductor materials are used to purify water. These photocatalysts, when appropriate rays fall on them, degrade the biological pollutants present in the water. This method is characterized by its effectiveness and high efficiency. As it is an inexpensive method and, in most cases, solar radiation is used as a source of stimulating rays. Studies are still ongoing to increase its efficiency and effectiveness (X. Chen, 2020). Figure 1.1 shows the photocatalysis mechanism diagram.

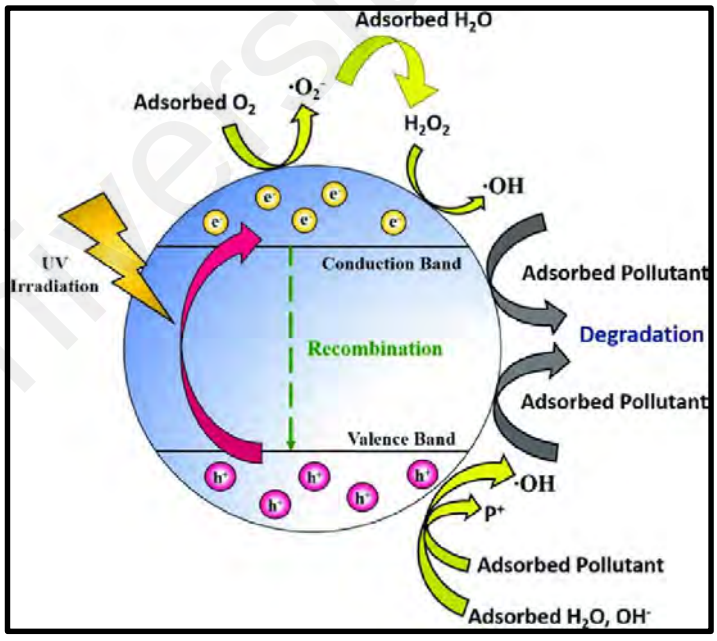

Figure 1.1: Photocatalysis mechanism diagram (Leong, 2018).

1.1.3 Zinc Oxide

Among the most widely used nanomaterials, zinc oxide (ZnO) has gained great interest in the scientific and medical communities, due to its important use in many biomedical and anti-bacterial applications, due to its chemical and physical properties, such as its high electrochemical correlation coefficient and photochemical stability (Borysiewicz, 2019). ZnO is classified as a semiconductor within the group (II-VI) between ionic and covalent semiconductors. ZnO can be found in one-dimensional, two-dimensional and three-dimensional structures (M. Kumar, 2010). ZnO shows wurtzite (hexagonal symmetry) or (cubic symmetry) rock salt structure, but ZnO crystals are more common and stable with wurtzite structure. There are several different methods for preparing ZnO NPs, including physical and chemical methods such as thermal evaporation, chemical vapor deposition (CVD), physical vapor deposition, sol-gel deposition, electrochemical precipitation and pulsed laser ablation (Ahsanulhaq, 2007; Al-Sabahi, 2016; Behera, 2018; Kamaruddin, 2010). Figure 1.2 shows the schematic diagram of the hexagonal wurtzite structure of ZnO.

The sedimentation method is one of the simplest and least expensive methods of preparing ZnO NPs. It is done by adding an amount of sodium hydroxide solution in droplets to aqueous zinc sulfate solution until the basic pH is reached, after which the process of washing and filtering the sediment for several times and then drying it for a period of time until it is obtained on a white precipitate of nanostructured ZnO (M. Kumar, 2010). ZnO is one of the most widely used semiconductors in various fields such as flat screens, electroacoustic devices and photocatalysis (Behera, 2018; Borysiewicz, 2019). ZnO is a wonderful material with multiple properties and is suitable for high technology such as light emitting diodes, optical

detectors, chemical and biological sensors, and energy collecting devices including solar cells, nanogenerators, electromagnetic, etc. due to high chemical and thermal stability, photoelectric and piezoelectric properties (Jorge, 2012; M. Kumar, 2010).

The use of nanostructured ZnO was not limited to these fields only, but it was an important element in the water treatments, especially in the past years. As it witnessed a remarkable development in the use of nanotechnology in medicine, where nanoparticles can be manufactured in the shape and size specified for the required purpose (Mabrouk, 2021; Norton, 2004). As there is a possibility of providing new methods of treating diseases that were difficult to focus on due to size restrictions, and the demand for environmentally friendly nanoparticles of metal oxides for pharmaceutical applications became increasing. There is an increasing need to search for alternative methods to formulate new types of antibiotics that are safe and cost-effective to eliminate and control pathogens (Ahsanulhaq, 2007). As most biological processes take place at the nanoscale level, joint efforts of nanotechnology and biology can solve important biomedical problems (Conradt, 2011).

Among the many semiconductors, ZnOs are biologically safe, cost-effective, non-toxic, and very beneficial against pathogenic bacteria (M. H. Huang, 2001). ZnO has received increased attention in recent years due to its stability under harsh environmental conditions and because zinc compounds are included in the Generally Recognized as Safe GRAS list (i.e. generally considered non-toxic and safe by the US Food and Drug Administration), ZnO-NPs are used in many industrial sectors (Zhou, 2017). Various medicinal products, such as medicines and cosmetics, are also widely used for treating a range of different skin diseases and for its inherent ability to absorb ultraviolet rays. It is used as a blocker of ultraviolet

rays in sunscreens. Antimicrobials and many medical products, studies also shown that ZnO-NPs can be highly toxic to cancer cells or bacteria and leukemia cells, and ZnO-NPs as compounds for drug delivery, gene delivery and bio sensing have also been studied for cancer treatment (Zak, 2012). ZnO has a wurtzite crystal structure (P63mc) at ambient conditions with a hexagonal unit cell as represented in Figure 1.2 and lattice parameters a = b = 0.3296 nm and c = 0.52065 nm (Wahab, 2011; Wan, 2013).

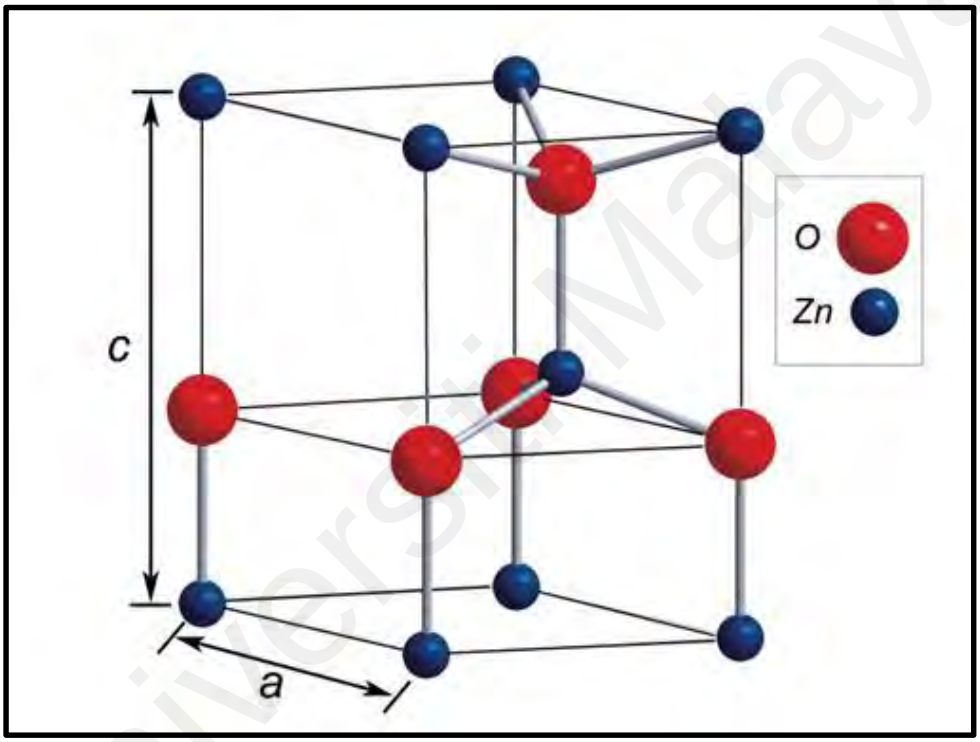

Figure 1.2: Schematic diagram of the hexagonal wurtzite structure of ZnO (Borysiewicz, 2019).

1.1.4 Optical properties

In addition to what was previously explained on the important properties of nanomaterials, these materials have captured the attention of researchers and scientists working in the field of optics, due to the unprecedented properties that these materials possess, as they differ in their optical properties from their counterparts of traditional large-grained materials (Zhang, 2009). It is surprising

that the effect of the size of the particles changes the optical properties of the material, including scattering or optical cracking of the surface of the material. For example, the known color of pure gold grains whose diameter is more than 200 nanometers is the golden-yellow color that we know, but if these grains are reduced to less than 20 nanometers, they are colorless (transparent) and with increasing reduction of the grains (Trotta, 2013). The grains appear in different colors from green to orange and then red, according to the dimensions of their diameters. The reduction in the sizes of the gold grains is reflected in the ability of these grains to resist photo-cracking and their combination of narrow-range spectral emission and an extensive excitation spectrum (I. Khan, 2017). Figure 1.3 shows the optical properties diagram. The field of electronics and optics is one of the most important areas of application for nanomaterials that combine optical properties and superior electrical conductivity in their properties. These materials are used in the manufacture of high-resolution, high-contrast and color purity screens, such as television screens and modern computers (Zhang, 2009).

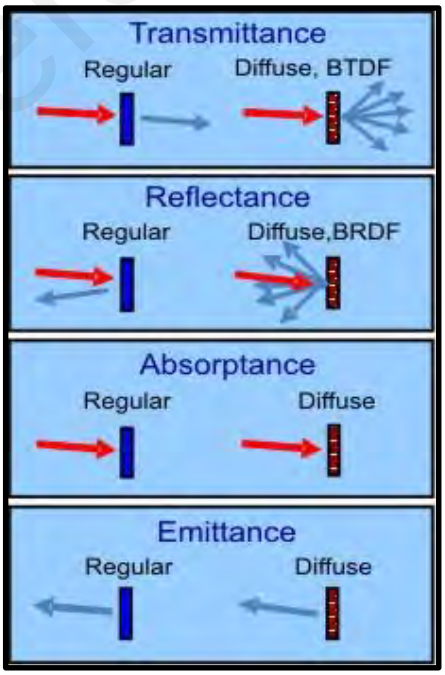

Figure. 1.3: Optical properties diagram.

1.1.5 Nanotechnology

Nano is a very small unit of measurement for dimensions. Where nanoscale equals one in a millionth of a millimeter (Abdulrahman, 2014). This means that it is impossible to see objects of this size with the naked eye or some simple magnifiers. Nanoscale used in atomic measurements in order to determine the dimensions of the particles in various materials (Helland, 2004). Accordingly, nanotechnology can be defined as the science that studies the possibility of changing matter at the nanoscale level (Morris, 2007). The importance of this technology lies in producing new materials or advanced devices to serve human interests in various fields. However, it must be noted that the term nanoscale is one of the old scientific terms that the scientist Richard Feynman addressed in 1959 during a lecture he gave at the American Physical Society; as he said there is a lot of space inside the atom, but the matter was not taken seriously at the time (Nouailhat, 2006; Runowski, 2014).

1.2 Research problem and motivation

Water pollution has been a necessary concern of the whole world due to water's importance in life. Water is vital to all forms of life, but it is also a valuable and unavoidable resource in a wide range of industrial processes. With the rapid development in various industries, it was matched by a significant increase in the number of internal origin pollutants of different nature in various water sources. These pollutants can cause significant health problems for humans and other organisms. As such, it is important to improve a technology that can monitor and treat these pollutants of all kinds.

In the last few years, many kinds of research have been conducted with various techniques in this field, including research related to the use of photocatalytic materials. That means when the light is used in combination with a catalyst, usually,

a semiconductor material such as zinc oxide (ZnO), radicals generated, and organic pollutants filtered as a result. In most cases, these photo-catalysts, which are metal oxides with a wide gap, can only be activated by high-energy ultraviolet (UV) radiation. This, in turn, may raise the cost incurred in the process, making it less feasible for large-scale photocatalytic applications. Therefore, a lot of research has been done to find ways to use solar energy to stimulate photosynthesis instead of ultraviolet radiation. Thus, the photo-catalysts had to modify to become active in the visible region of the solar spectrum.

ZnO is a promising semiconductor compound due to its various properties, such as its bandgap of 3.37 eV at room temperature and binding energy of 60 meV. ZnO is one of the most widely used in nano technique formation, such as nanowires, nanorods, nanotubes, and nanorings by different dopants materials. There are also many different methods for fabricating ZnO nanostructures, such as electrochemical deposition, pulsed laser deposition, chemical vapor deposition, and hydrothermal method. It is possible to change the optical characteristics, structural and electrical properties of ZnO by doped with an element of the group III such as Al, Ga, and In. Each of these elements is characterized by having three valence electrons and can form a shared pair with the ZnO. In this research, ZnO is doped with Ga and fabricated by the hydrothermal method to form nanorods. Ga has high conductivity and low reactivity. It also has resistance to oxidation. The Ga-doped ZnO increased electron mobility because the covalent bond length of Ga-doped is very close to that of Zn-O. It also reduced electrical resistivity.

This searches for new materials with improved physical-chemical properties that monitor and treat these pollutants of all kinds an urgent necessity. Doping ZnO nanostructures with an element of group III such as Al, Ga, and In can improve the

photocatalytic degradation of contaminants and the ZnO material's antimicrobial activity. In this work, Ga doped ZnO nanorods with different percentages (0%, 0.5%, 1%, 3% and, 5%) were synthesized and supported in glass substrates by a fast-hydrothermal microwave heating synthesis. According to the Ga-doped percentage, the morphologies, diameters, and lengths of Ga-ZnO nanorods are characterized and found to vary significantly.

1.3 Research objectives

The objectives of this study are:

1. To prepare the Ga-doped ZnO nanorods via microwave-assisted method.
2. To describe the properties of Ga-doped ZnO nanorods.
3. To use Ga-doped ZnO nanorods for photocatalytic application.

1.4 Scope of study

In this work, a facile and rapid microwave-assisted method is used to synthesis a different percentage of Ga-doped ZnO nanorods. Ga doping is expected to enhance the morphological, structural, optical and photocatalytic properties of the ZnO nanorods. Ga doping has been shown to possess a high conductivity, low reactivity, and resists oxidation (Alexandrov, 2020; Hong, 2010; Muchuweni, 2016a). The Ga-doping can increase electron mobility since Ga covalent bond lengths are very close to Zn-O and reduced electrical resistivity (Y.-Q. Li, 2010). Herein, Ga-doped ZnO nanorods with different percentages (0%, 0.5%, 1%, 3% and, 5%) of Ga are synthesized and supported in glass substrates by a microwave-assisted method.

1.5 Thesis framework

This thesis consists of five chapters. In the first chapter, a background is presented on the main themes of the thesis, namely water pollution, methods of eliminating water pollution, zinc oxide, photoelectric properties and nanotechnology. As mentioned in the first chapter as well as research problems and motivation, research objectives, the scope of the study and thesis framework. While the second chapter dealt with the literature related to this thesis, such as the work done in the purification of water pollution with its various techniques, the nanomaterials, its classification, and its properties, ZnO fabrications, microwave-assisted method, ZnO doping, gallium-doped ZnO and photocatalysis. Chapter 3 presents a methodology to construct ZnO and GZO nanorods in which this study employs microwave-assisted methods. Chapter 4 shows the results and discussion of hexagonal wurtzite Ga-doped ZnO, the response of NRs during the photocatalytic process, the results of ZnO and GZO nanorods morphology, crystal properties, functional groups, optical properties, and photocatalytic activity. Finally, Chapter 5 summarizes the fabrication technique with conclusions, future works, and recommendations.

CHAPTER 2: LITERATURE REVIEW

2.1 Nanotechnology in Water Pollution Remediation

The use of nanotechnology in water treatment is one of the modern methods of wide demand and steady development. There are many different types of research related to the use of nanotechnology in water treatment and there are many different methods that have been worked on recently. All of these methods use nanotechnology from the use of nanomaterials but differ in their properties, advantages and objectives. One of these methods is the nano-adsorption method, which focuses on the adsorption of pollutants by solid surfaces (Schwarzenbach, 2012). In it, nanomaterials are used that can absorb organic and inorganic pollutants present in water. These materials should have such characteristics as small volume, catalytic capacity, high reactivity, large surface area, ease of separation, and a large number of active sites to interact with various pollutants present in the water. However, this technology is considered high cost in terms of production (Xingjian, 2018).

Also recently appeared the method of nano-metals and nano-metal oxides for the treatment of water pollution. This method is used as a filter for media, slurry reactors, powders and pellets. It treats water from heavy metals and radionuclides by not allowing it to pass through. However, a disadvantage of this method is that it is not reusable and ineffective in treating fine compounds. Another modern method of water treatment is the use of membranes. This method is represented in the use of nanoporous materials with thin layers that allow water molecules to pass through while preventing the passage of some other particles such as bacteria, viruses, salts and minerals (Xingjian, 2018). This method requires high pressure to ensure the passage of water through these membranes. Research in this method is

ongoing to improve the permeability of these materials and make them more effective. One of its disadvantages is that it needs a high power source. Disinfection and microbial control are methods of nanotechnology in water treatment. In this method, non-toxic nanomaterials are used to treat water and get rid of microbes such as TiO_2, Ag nanoparticles, ZnO nanoparticles and carbon nanotubes. However, one of the disadvantages of this method is its weakness in getting rid of the various substances present in the water (X. Chen, 2020).

One of the easiest ways to use water is a photocatalytic activity in UV and possibly visible light range. Which depends on the manufacture of nanomaterials that can degrade the organic pollutants present in the water. These materials use incident light to form a reaction that degrades these compounds into environmentally friendly compounds. This method is inexpensive and does not require a source of energy, as the source is solar radiation. It also does not require or include toxic or harmful substances (Sulaiman, 2022).

2.2 Nanomaterials

Nanomaterials are the building materials for the twenty-first century and its basic building blocks and the important pillar of the twenty-first century technologies (nanotechnology, biotechnology, information and communication technology), which is considered a criterion for the progress and civilization of nations and an indicator of their renaissance (Zhao et al., 2018). It was discovered in ancient Egyptian history their use of nanomaterials, such as the blue color produced by a mixture of glass and quartz (Johnson-McDaniel, 2013). The Roman civilization's use of nanomaterials has also been documented by their use of Lycurgus cups, which are dichroic glass displaying different colors (Schaming, 2015). The use of nanomaterials also appeared by the Mesopotamian civilization in the use of glazed

porcelain for metallic luster decoration (Artioli, 2007). While the first scientific description was reported by the scientist Michael Faraday in 1857, which is the synthesis of a colloidal Au nanoparticles solution (Brun, 1991). In 1908 Mie put an explanation behind the specific colors of the metal colloids (Mie, 1908). From then and in the 1940s, SiO_2 nanoparticles were synthesized as substitutes for carbon black to strengthen rubber (Mindy, 1998). Among the most important achievements in nanomaterials was when Samsung introduced anti-bacterial technology.

In 2003, it was launched under the Silver Nano™ brand name in their washers, air conditioners, refrigerators, air purifiers, vacuum cleaners, which use ionic Ag nanomaterials (Samsung, 2011). In the same year, Mercedes-Benz also introduced a car containing a transparent film based on nanomaterials in series production for both metal and non-metallic paint finishes (Malsch, 2005). In addition, the first major commercial use of dye-based solar cells was when Logitech in 2012 brought an external light-powered iPad keyboard to the market (Kreuter, 2006). In 2014, about 1814 nanotechnology-based consumer products were commercially available in over 20 countries all over the world (Vance, 2015). Nanomaterials vary in terms of source, as they differ according to their proportions, such as whether they are organic or inorganic materials, or natural or synthetic materials. This is considered all kinds of well-known engineering materials such as metal and metal alloys, semiconductors, oxides and metals, as well as in this century and enhanced performance in an unprecedented manner (Mohapatra, 2020; Runowski, 2014). Nanomaterials are classified according to their structure into four categories as shown in Figure 2.1: (1) zero-dimensional (0D), one-dimensional (1D), two-dimensional (2D) and three-dimensional (3D) nanomaterials (Mohapatra, 2020). In one-dimensional nanomaterials two dimensions are at the nanoscale (x,y) and the

other is outside the nanoscale. This structure appears as a needle shaped nanomaterials like nanofibres, nanotubes, nanorods, and nanowires (Liu, 2013).

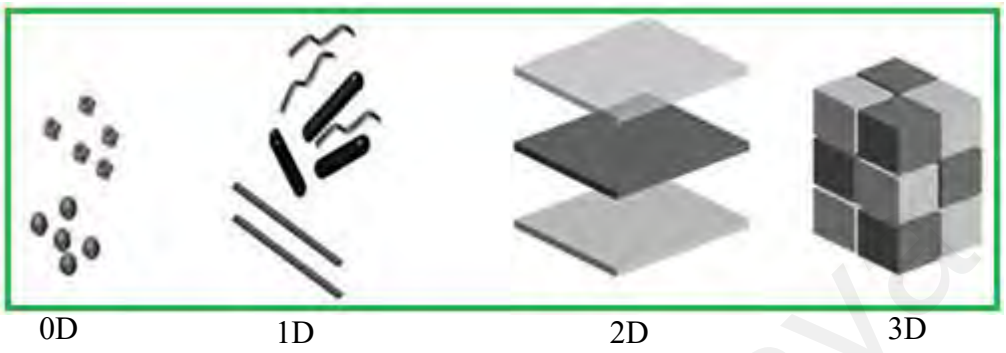

Figure 2.1: Classification of Nanomaterials. (Mohapatra, 2020)

2.3 Zinc Oxide Fabrication

2.3.1 General Methods for Fabricating Zinc Oxide

Over the past decades of development in the field of materials science engineering, many scientists have tried to improve the shape and size of nanostructures of materials in their research. From this point on, many tremendous efforts have been directed and expended in various researches to investigate the undiscovered characteristics of heterostructures/different types of semiconductors materials such as ZnO, SnO_2, TiO_2, etc (Arakha, 2012; Buzea, 2007). These heterostructures include nanorods, nanotubes, nanowires, nanobelts, nanoflowers, nanosheets, nano urchin-like structures and other structures that can be formed. In particular, among these compounds, ZnO is considered one of the most promising semiconductors due to its chemical stability, photosensitivity, fast electron transfer ability, and better light absorption compared to TiO_2 (Behera, 2018). There are many different techniques for fabricating ZnO nanostructures, and they can be divided into two

general methods. The first method can be called a bottom-up approach, and the second method is called a top-down approach (Al-Sabahi, 2016; Rajendra, 2013). The first method can be defined as building the nanostructure based on the interaction of inner-molecules in the material, while the second method is defined as by carving the materials to the desired final shape, as is the case in lithography (H.-C. Cheng, 2006).

2.3.2 The Template-Assisted Technique

According to recorded information in the Web of Science data source, S.Hingorami has reported the first syntheses of ZnO nanostructures. They obtained ZnO-NPs in the size range of 5-40 nm by microemulsion-mediated method (S.Hingorani, 1993). About 2 years later, Elshall prepared ZnO-NPs using laser ablation method using Zn target (Elshall, 1995). In this time there are many techniques that are used to build nanostructures of many different materials to improve their different properties. Among these techniques that can be mentioned here are template-assisted method, dip-coating and immersion, spin-coating, electrochemical deposition, sol-gel, and chemical vapor deposition (CVD) (Borysiewicz, 2019; Chen, 2011; Jimenez-Cadena, 2010). Muni Raj Maurya et al have used a soft template-assisted method to synthesize the ZnO by precipitating it inside the alumina template. Well separated and vertically aligned growth of the synthesized nanowires has been synthesized which in turn give a fast response to the UV photodetector (Maurya, 2019). Usually, in fabricating the ZnO via a soft template-assisted method, two aluminum plates are used in oxalic acid. The molten zinc is then poured into the alumina nano-mold. Homogeneous and structured nanowires obtained from this method have a good potential for use in practical electronic applications (Vivekanandan, 2020).

2.3.3 The Dip-Coating Technique

In addition, the dip- coating method has been used by coating glass plates by dipping for 30 seconds in the prepared coating solution containing ZnO and curing at 80°C for two hours. Nanoparticles with a hierarchical and hexagonal structure obtained from this technique show good photocatalytic properties (Khorshidi, 2021). ZnO doped with aluminum can be achieved by coating the glass plates by repeatedly dipping them on the prepared coating solution containing ZnO doped with aluminum and then placing them in a plate that is heated to a temperature of 250 °C for 10 minutes. A hexagonal crystal structure can have a slight influence on the energy bandgap (Urper, 2020).

2.3.4 The Spin-Coating Technique

The spin-coating method is used to form ZnO nanoparticles in fabricating the solar cells with efficiency is increased via this method (Dehghan, 2019). Thin-film samples of ZnO appeared in the form of amorphous grains, showing a high photo-response (Park, 2018). The spin-coating method has successfully formed ZnO doped with gallium and indium which perform the outstanding electrical and optical properties of high sensitivity to lighting applications (Karabulut, 2021). The electrodeposition method has previously been used to form the well and evenly silver-doped ZnO nanorods and silver-doped ZnO nanoparticles on FTO glass. The process is done by electrolysis of a solution containing ZnO compound by applying a high voltage to it for a certain period time (Rasouli, 2018).

2.3.5 The Sol-Gel Technique

On the other hand, other groups have been able to fabricate a sun-sensitive amorphous carbon with ZnO to form a solar-sensitive diode using electrochemical

deposition technology (Koc, 2018). Using sol-gel technology, one can manufacture a new acetic acid-targeted gas sensor designed with new ZnO foam as a sensor material. Citric acid is added to zinc nitrate solution with continuous magnetic stirring to form a colorless solution. The solution is heated to form a gel and then placed in ceramics and heated to form a foam. A new gas sensor for acetic acid is created with the unique ZnO foam as the sensing material shows promising and distinctive property (Han, 2019). ZnO nanoparticles are synthesized using sol-gel technology to create an electrode material in an electric cell. Zinc acetate is added to sodium hydroxide and polyethylene glycol and then heated in the solution until boiling. After cooling, nitrite acid is added and after filtering and precipitation, it is heated to obtain ZnO nanoparticles. This method can manufacture a supercapacitor cell using an improved electrolyte of zinc nanoparticles which showed good capacitive behavior relatively higher specific capacitance value of up to 118.12 mF can be considered a promising candidate as electrode material for application in supercapacitors (A. Kumar, 2020).

2.3.6 Chemical Vapor Deposition Technique

Among these techniques, chemical vapor deposition technique is the most widely used in the treatment of various materials such as ZnO. This technique can be summed up as coating thin layers on surfaces (substrate). It is a technique in which a film of material is deposited from a steam lump by chemical decomposition on the base of a substrate (Jin, 2018). This technology is often thermally driven. Film deposition is controlled by a chemical reaction between materials. As a result, this technology is more versatile than many different technologies. One of the advantages of this technique is growth under unbalanced preconditions and the nature of the precursor chemical can in principle be used to manage and shape the

deposited piece. There are many other benefits of the approach from a viable per-growth conformational process and large area growth, yield opportunity, repeatability, and very high purity in the cultured material (Kamaruddin, 2010). Aluminum-doped ZnO porous thin films have been developed for thermoelectric applications using chemical vapor deposition technology. It enables the electrical conductivity and power factor to be increased and maintain the low thermal conductivity of these thermoelectric films (Saini, 2019). In addition, high conductivity films of ZnO doped with different percentages of gallium using vapor chemical deposition technology have been shown. The optical transparency at visible wavelengths was above 80% for all films formed. This in turn made these films highly suitable for TCO applications (ponja, 2020). **Fig. 2.2** shows the schematic diagram of the chemical vapor deposition technique.

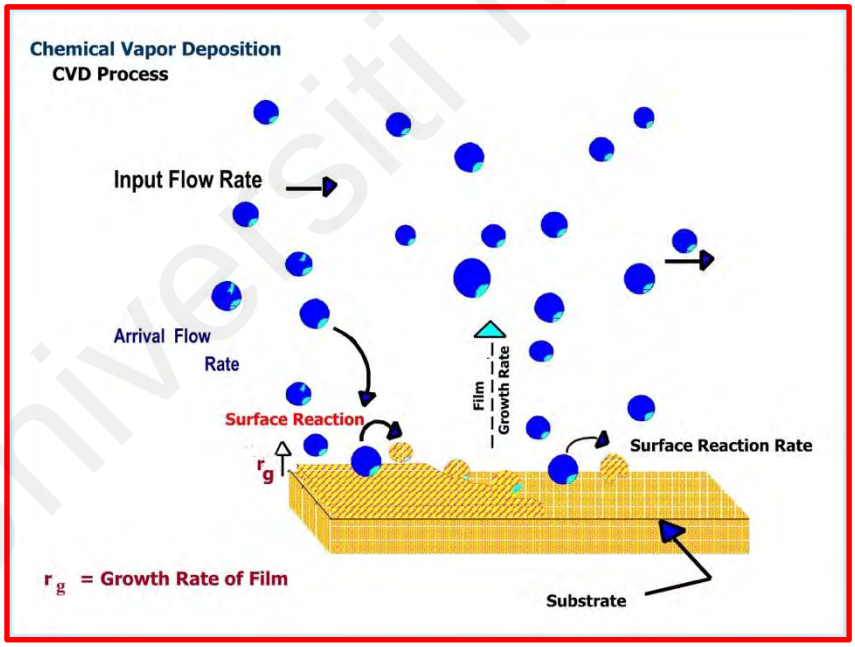

Figure 2.2: Scheme of the chemical vapor deposition technique (Cai, 2021).

2.4 Microwave-Assisted Method for Synthesis Nanomaterials

Microwave chemistry is the science concerned with the study of the application of microwave irradiation to various chemical reactions. This process depends on the effective heating of the material by microwave dielectric heating (Aldossary, 2015). It also depends on the ability of a specific material (e.g., solvent and/or reagents) to absorb microwave energy and convert it into heat (B. Chen, 2014). While in liquid phase synthesis of different nanomaterials such as ZnO, microwave irradiation leads to heating of two main mechanisms, namely dipole polarization and ionic conduction. **Fig. 2.3** shows a microwave-assisted method diagram. Microwave-assisted synthesis is a unique, simple and rapid technology that is used to process materials of higher reproducibility quickly and efficiently (Dai, 2006). This method has emerged as an economical tool for particle size reduction and solubility enhancement. This method is also environmentally friendly and effective for preparing various combinations such as discs, agglomerates, gel granules, nano-systems, microspheres, film coatings, and solid dispersions (Gawande, 2014).

Microwaves are electromagnetic radiation and are located between the infrared region and radio waves in frequency and wavelength as their wavelength lies between 0.01 and 1 meter. These waves induce the nucleation or growth of matter. In general, microwaves interact with polar molecules, so that this interaction leads to the rotation of polar molecules and moves them with a vibrational movement, and it also generates heat inside the material (Grewal, 2013; X.-Y. Huang, 2017). The microwave-assisted method has been widely used in the preparation of ZnO nanorods recently. Its synthesis has advantages over all other methods because it is more energy efficient and it can lead to improve isolated yields of products with green synthesis (Grewal, 2013; Majeed, 2017). The microwave-assisted chemical

reduction technique is used to deposit silver and ZnO nanoparticles on the surface of reduced graphene oxide at different weight ratios and is used as antibacterial (Yi-Huang, 2019). Microwave-assisted technology has also been used to prepare highly dispersed suspensions of ZnO nanoparticles, which can be used as a tissue repair material and reduce the side effects of the embedded particles (Manuja, 2020). Among the uses of microwave-assisted technology is to synthesize ZnO nanorods doped with manganese for the production of semiconductor detectors. The manufactured devices showed a high response to ultraviolet radiation and showed almost no response to the visible spectrum (Hussein, 2020). This technique is also used to synthesize ZnO nanorods for use in making a paper biosensor aimed at enhancing the convenience of monitoring doping concentrations (Yu-Hsuan, 2021). This technique is also used in the manufacturing of the ZnO nanoparticles using ascorbic and used as antibiotics. Antimicrobials and nanoscale biofilms of ZnO nanoparticles synthesized in this way are applied against Salmonella typhimurium, Klebsiella spp. It was noted that they have shown excellent results (Kazi, 2020).

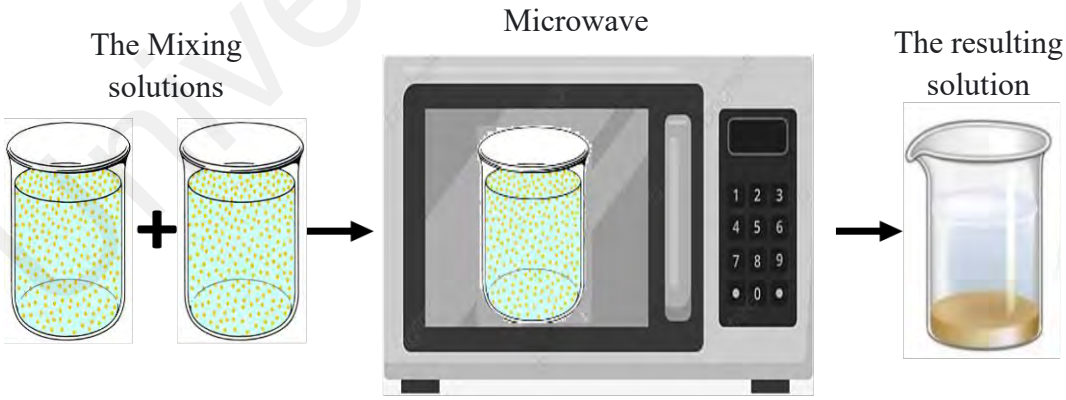

Figure. 2.3 Microwave-assisted method diagram.

2.5 Zinc Oxide Doping

Adding some impurities to the pure semiconductor, such as ZnO, is called doping. The impurities create new energy levels that fall into the forbidden gap between the

conduction and valence bands. The grafted semiconductor is classified into two types according to the type of impurities added to it, the first type, which is a semiconductor (n-type) (Norton, 2004). It is called the negative type because the majority charge carriers are electrons and the minority charge carriers are holes, and this type is obtained by adding donor impurities to a pure semiconductor (Zak, 2012). This type of conductivity is relatively easy to realize via excess Zn or with Al, Ga, or In doping (Alexandrov, 2020). Many recent studies used ZnO doping with these materials, Al, Ga, and In in order to improve its properties (Wahab, 2011). These elements are characterized by having three valence electrons and can form a shared pair with the ZnO (Zhou, 2017). Among these elements, Ga offers various advantages such as: close atomic radius of Ga and Zn, leading to minimal strain and local lattice distortion (S. Yang, 2011). Ga-doped ZnO has been successfully grown in wurtzite nanorods structure with the improvement in electrical, optical properties and photosensitivity (Hsiao, 2013; Iwantono, 2016; S. J. Young, 2016). The increase in the Ga doping concentration has caused the average diameter of the nanorods to decrease slightly, increase in the FWHM, dislocation density and decrease in mean grain sizes (Lee, 2012; Muchuweni, 2016b).

The other type is called a p-type semiconductor with most charge carriers are the holes. As for the Fermi level in the doped semiconductors, it approaches the conduction band when it is a n-type semiconductor, but behave differently when it is a p-type semiconductor (Tian, 2018). ZnO thin films when doped with titanium gives a noticeable effect on their structural, morphological, and optical properties. A change in the bandgap has been observed which made these films useful for optoelectronic applications (Ramesh, 2021). On the other hand, doping of ZnO with aluminum has attracted much research and is very extensive. Among these

researches is the use of aluminum-doped ZnO thin films in the preparation of photocatalysts (Majdi, 2021). Among the uses of ZnO nanoparticles doped with aluminum are the devices used in sensing sensitive materials such as the acetone sensor. It is reported that it greatly improves the acetone sensing properties of the sensors (Yang, 2020). The indium must also be mentioned, as it has been used in many different studies. Including the use of ZnO nanowires doped with indium in X-ray sources and detectors. These wires show a distinctive effect in the process of X-ray detection (Yangyang, 2021). There is also the use of ZnO nanoparticles doped with indium to manufacture an electronic transport layer, which is used in the manufacturing the inverted solar cells. Solar cells that are fabricated from this layer consisting of ZnO nanoparticles doped with indium have a high energy conversion efficiency and an improvement of about 40% compared to the device made from a layer of pure ZnO particles (Luo, 2021).

As for the element of gallium, which is the element that is used in this current study, ZnO nanoparticles doped with gallium has seen to benefit in anti-bacterial applications. It has been used against different types of bacteria such as Escherichia coli, Klebsiella pneumoniae and Staphylococcus aureus. These antibiotics are shown to be effective in enhancing antibacterial activity (Sathish, 2021). Gallium-doped ZnO nanoparticles are used in the fabrication of substrates based on the contribution of EM enhancement to surface plasmon resonance (SPR). It shows that the feasibility of using gallium in EM contributions to SERS using semiconducting substrates could contribute to the development of this type of semiconductor (Wang, 2021). Gallium-doped ZnO thin films have been used in the manufacture of coatings with properties of low-emissivity coatings that exceed industrial and environmentally friendly standards. It has been determined that it can be used as a cheap, effective and easy-to-production alternative (Clara, 2020).

2.6 Gallium-doped Zinc Oxide

Fig. 2.4 shows the schematic diagram of Ga-doped ZnO. Gallium is located in the general periodic table of the elements in the boron family (group 13), which includes the semi-metallic boron (B), and metals such as: aluminum (Al), gallium, indium (In), and thallium (Tl), and all of these five elements have three electrons in its outer energy level. Gallium is easily associated with many metals, and is commonly used in the manufacture of alloys that melt at low temperatures (Stepanov, 2016). It is one of those four metals that include: (mercury, rubidium, cesium), which exist in the liquid state at a temperature approaching room temperature, of these four metals, gallium is the least reactive and toxic; Therefore, it is considered the safest and most environmentally friendly option. To be used in the manufacture of thermometers, barometers, and heat transfer systems, whether cooling or heating devices (Helen, 2012).

Gallium has atomic weight of 69.723, atomic radius of 126 pm, radius of Ga^{+} ion 113 pm, ion radius of Ga^{+3} 62 pm, principal oxidation number +3. The wavelength corresponding to the two main lines of its spectrum (in centimeters x 810) is 4172.2 and 4033.2. Gallium reacts from oxygen to produce gallium oxide according to the following equation (S. Kumar, 2013):

$$4Ga + 3O_{2(g)} \longrightarrow 2Ga_2O_3 \qquad (2.1)$$

While gallium reacts with water to produce gallium hydroxide, as in the following equation (S. Kumar, 2013):

$$2Ga + 6H_2O \longrightarrow 2Ga(OH)_3 + 3H_2 \qquad (2.2)$$

Gallium can enter the zinc oxide matrix by replacing the Zn^{+2} due to the convergence of the ionic radii between them. Gallium adds an electron to the matrix

because of the difference between its reaction numbers Ga^{+3} and that of Zn^{+2} (Park, 2018). It was formed from previous research that with increasing Ga dopant concentration, the sharpness and intensity of XRD peaks showed a decrease, corresponding to the decrease in the average crystallite size (Park, 2018). This was explained that Ga^{+3} ions entered the crystal lattice of ZnO to replace the Zn^{+2} (X. Li, 2016). It was also found from previous research that gallium enhanced the optical properties of zinc oxide by affecting the number of charges carrier (Shtepliuk, 2020).

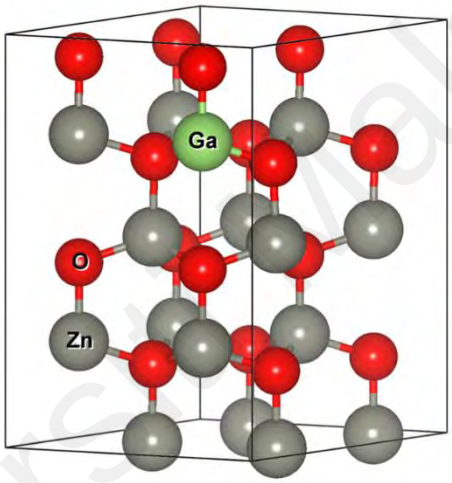

Figure 2.4: Schematic diagram of the Ga-doped ZnO (Sikam, 2019).

2.7 Photocatalysis of ZnO Nanoparticle

In the last few years, many kinds of research have been conducted with various techniques in this field, including research related to the use of photocatalytic materials. That means when the light is used in combination with a catalyst, usually, a semiconductor material such as ZnO, radicals are generated, and organic pollutants are filtered as a result (Murali, 2018). **Fig. 2.5** shows the schematic diagram of the ZnO photocatalytic. The photocatalysis started in 1911 when Alexander Eibnor used a technique to bleach dark blue pigment by using ZnO in the presence of sunlight. After that, Kozak and Bruner wrote an article in which

they discussed the breakdown of oxalic acid using a photocatalyst in 1913. In 1921 photocatalysis was used to formaldehyde using a photocatalyst (ferric hydro-oxide and colloidal salts of uranium). TiO_2 was discovered in 1938 and used as a photocatalyst for bleaching dyes. TiO_2 and ZnO have first observed to possess a photo-oxidation in isopropanol in 1964. In addition, electrochemical photolysis of water using platinum and titanium di-oxide electrodes have also been observed (Tahir, 2020).

In most cases, these photocatalysts, which are metal oxides with a wide gap, can only be activated by high-energy ultraviolet (UV) radiation. This, in turn, may raise the cost incurred in the process, making it less feasible for large-scale photocatalytic applications (Mamat, 2011). Therefore, a lot of research has been done to find ways to use solar energy to stimulate photocatalysts instead of ultraviolet radiation. Thus, the photo-catalysts have to be modified to become active in the visible region of the solar spectrum (Rajendra, 2013). This technique has been used in water treatments. Where these materials (photocatalysts) are used to purify water until it becomes suitable for human use. Many researches have been conducted to obtain the best materials in water purification by photocatalytic performance (Tahir, 2020). To obtain a good material that can degrade the organic water contaminants in the presence of visible light, the energy band gap must be less than 3.5eV. Gallium-doped zinc oxide (GZO) is considered as one of the photocatalyst materials that can give the good results in water purification.

Many researches have been conducted in this regard, and the difference lies in the percentage of Ga-doping and method of synthesis (Tahir, 2020). GZO thin films have previously been synthesized via spray pyrolysis technique with the recorded energy bandgap of ~3.26eV (Muchuweni, 2016b). By the sol-gel spin-coating

method, the prepared GZO thin films have the energy bandgap of ~3.28eV (Gupta, 2019). This energy bandgap value has been further reduced to 3.24eV with the GZO nano pagodas by atomic layer deposition technique (Chiu, 2015).

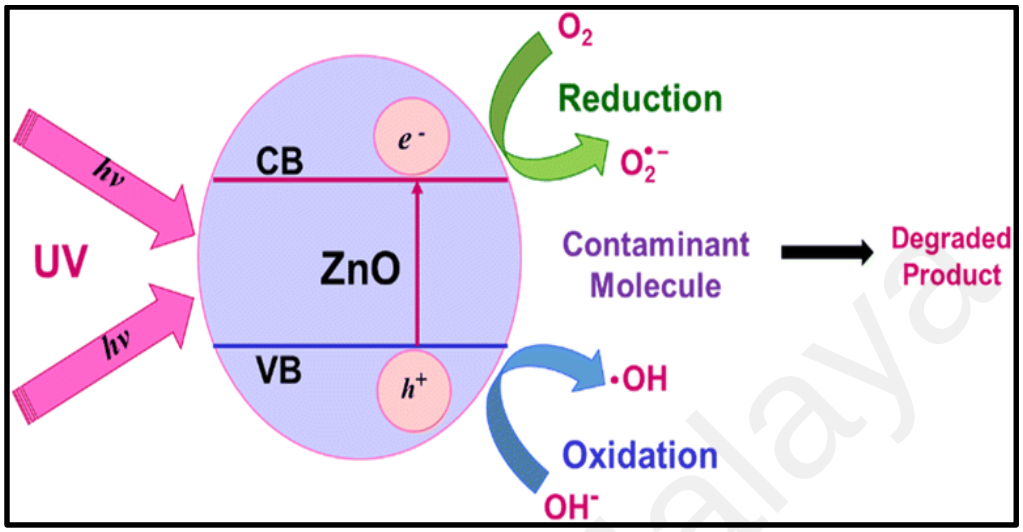

Figure 2.5: Schematic diagram of the ZnO photocatalytic (Farsi, 2021).

CHAPTER 3: METHODOLOGY

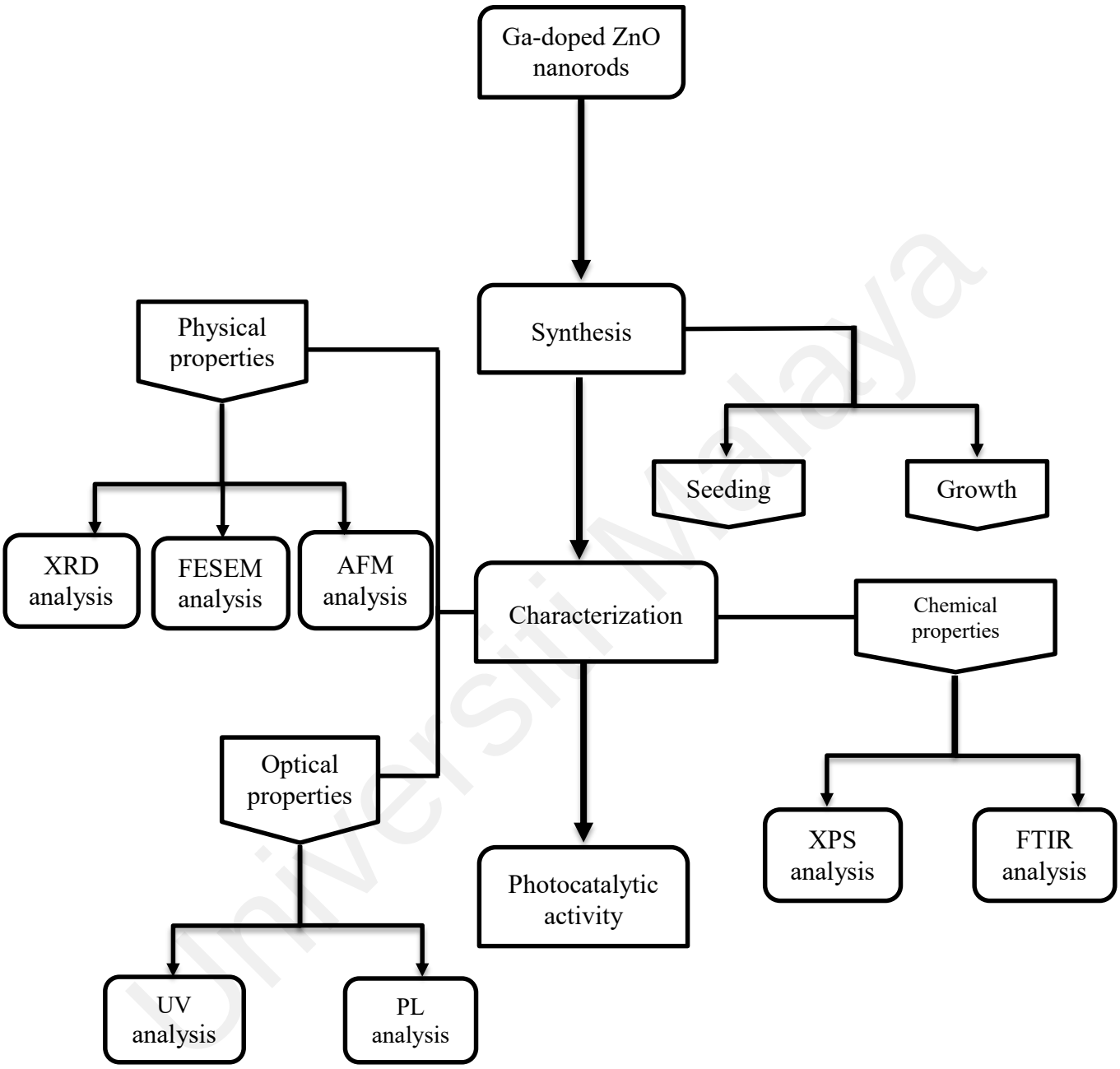

Figure 3.1: Research Flowchart.

3.1 Synthesis of Ga-doped ZnO Nanorods

Synthesis of the ZnO and GZO nanorods process was carried out in several different steps, namely, the preparation of materials, seeding preparation, and growth process. **Fig. 3.2** shows the schematic diagram of the ZnO and GZO fabrication steps.

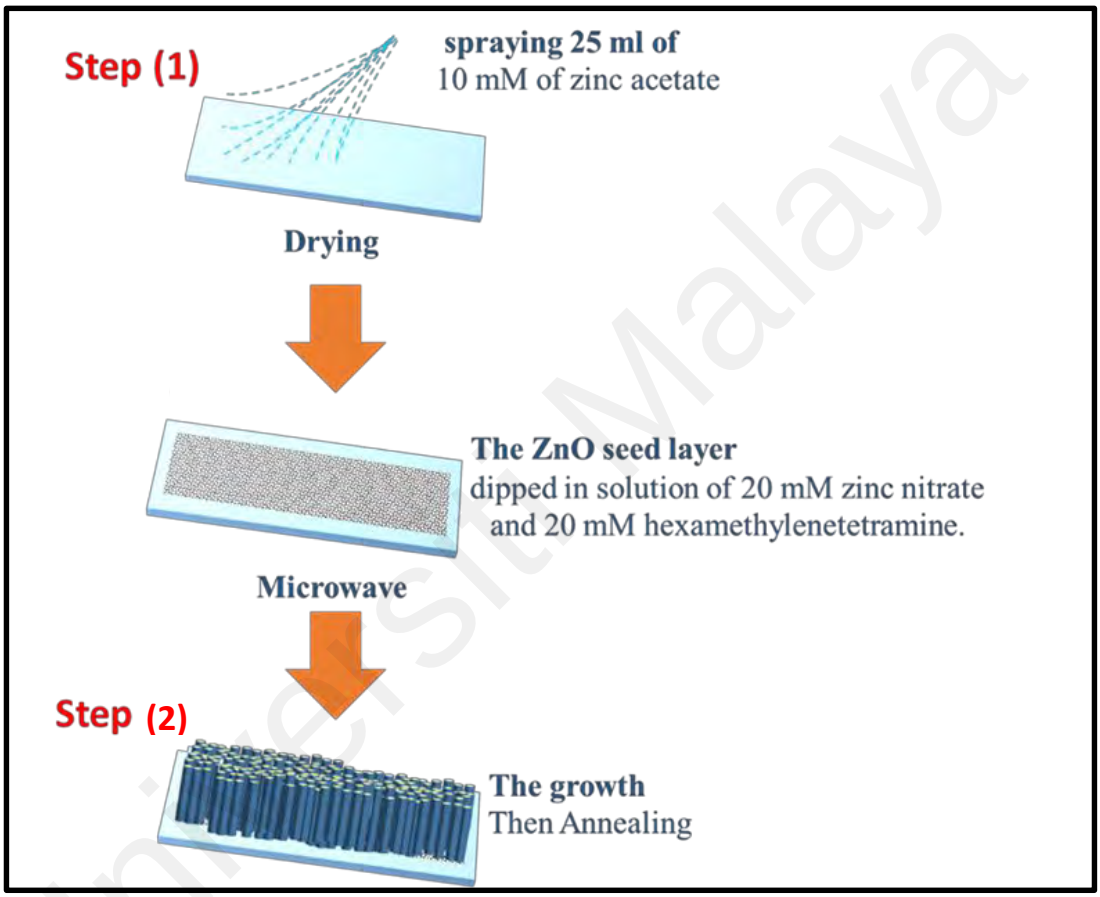

Figure 3.2: Schematic diagram of the ZnO and GZO fabrication steps.

Materials such as zinc acetate dihydrate, $Zn(CH_3COO)_2.2H_2O$ (Sigma Aldrich, USA), gallium nitrate, $GaNO_3$ (Merck, USA), hexamethylenetetramine, $C_6H_{12}N_4$ (Sigma Aldrich, USA), and zinc nitrate hexahydrate, $Zn(NO_3)_2.6H_2O$ (Ajax Finechem, Australia) are used as received without further purification. **Fig. 3.3(a)-**

(d) shows the photograph of different chemicals used in this study. Glass slides 7.5 cm long, 2.5 cm wide and 1 mm thick were used as substrates.

Figure 3.3: Photograph of different chemicals of (a) zinc acetate, (b) gallium nitrate, (c) hexamethylenetetramine and (d) zinc nitrate hexahydrate.

3.1.1 Seeding Preparation

For seeding preparation, glass substrates were pre-cleaned by successive sonication in soap water, ethanol, acetone, and deionized (DI) water for 15 minutes each. Then, the substrates were placed in an oven at 90^0 ℃ for drying. Seeding solution with a concentration of 10 mM was prepared by mixing zinc acetate dihydrate and gallium

nitrate in 25 ml of DI water with different doping percentages of 0.0%, 0.5%, 1.0%, 3.0%, 5.0%, labeled as GZO0, GZO0.5, GZO1, GZO3, and GZO5, respectively. The seeding layer deposited on cleaned substrates using the spray pyrolysis technique of seeding solution. A spraying rate of 1 mL/min (from a distance of 20 cm) was applied on the pre-heated substrates at 400 ℃ by gently moving it left and right for about 30 min. **Fig. 3.4** shows the photograph of the ZnO seeding preparation apparatus.

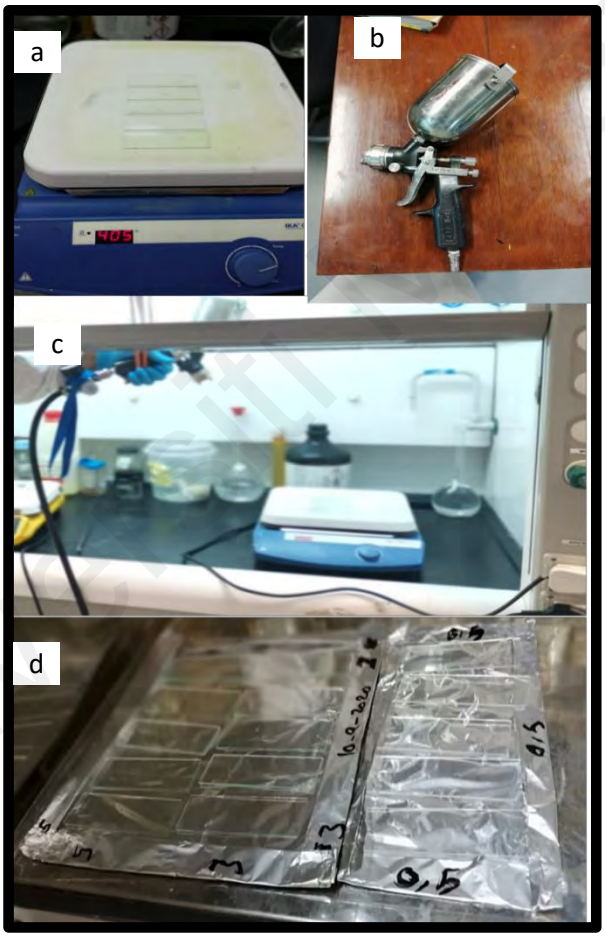

Figure 3.4: ZnO seeding preparation apparatus (a) The glass substrates were placed in an electric heater at 400 ℃, (b) The seeding solution were put in a spray device, (c) Spraying process was applied on the pre-heated substrates, (d) Glass slides after spraying.

3.1.2 Growth Process

The growth solution with a concentration of 20 mM was prepared by mixing zinc nitrate hexahydrate and gallium nitrate in 500 ml DI water with different doping percentages (0.0%, 0.5%, 1.0%, 3.0%, 5.0%)3. 100 ml hexamine will then be mixed in the DI water. The growth process of Ga-doped ZnO nanorods is performed by a microwave-assisted method shown in **Fig. 3.4**. First, the growth process is performed by the microwave method on the seeded substrates. Second, the seeded substrates are subsequently placed in a bath containing a growth solution. The chemical bath was heated in a commercial microwave oven (Panasonic, Low Mode) for 4 h, in which the precursor solution was renewed every 45 minutes. Finally, the growth was completed by annealing the growth substrates at 550 ℃ for 60 min.

ZnO NRs were grown by the following chemical reactions:

$$Zn(NO_3)_2 \longrightarrow Zn^{+2} + 2NO_3 \quad (3.1)$$

$$(CH_2)_6N_4 + H_2O \longrightarrow 6HCHO + 4NH_3 \quad (3.2)$$

$$H_2O \longrightarrow H_3O^+ + OH^- \quad (3.3)$$

$$Zn^{+2} + 2OH \longrightarrow Zn(OH)_2 \quad (3.4)$$

$$Zn(OH)_2 \longrightarrow ZnO(N_{rs}) + H_2O \quad (3.5)$$

Zn^{+2} and OH^- ions were produced from the ionization process of $Zn(NO_3)_2$ and NH_3 in the aqueous solution and the $Zn(OH)_2$ was precipitated in the aqueous solution. Part of the compound produced from this reaction, which is $Zn(OH)_2$ was slowly dissolved in the solution while the other part reacted slowly with the OH^- ions to form complex units of $Zn(OH)_4^{-2}$ (Santibenchakul, 2018). This process is done with the assist of microwaves as well as the spin process, which facilitates the disintegration of molecules as well as their association with each other. As a result,

the complex units of $Zn(OH)_4^{-2}$ absolutely decompose to form nuclei of ZnO which gather to ZnO nanostructures (S.-J. Young, 2016). **Fig. 3.5** shows the growth process of ZnO.

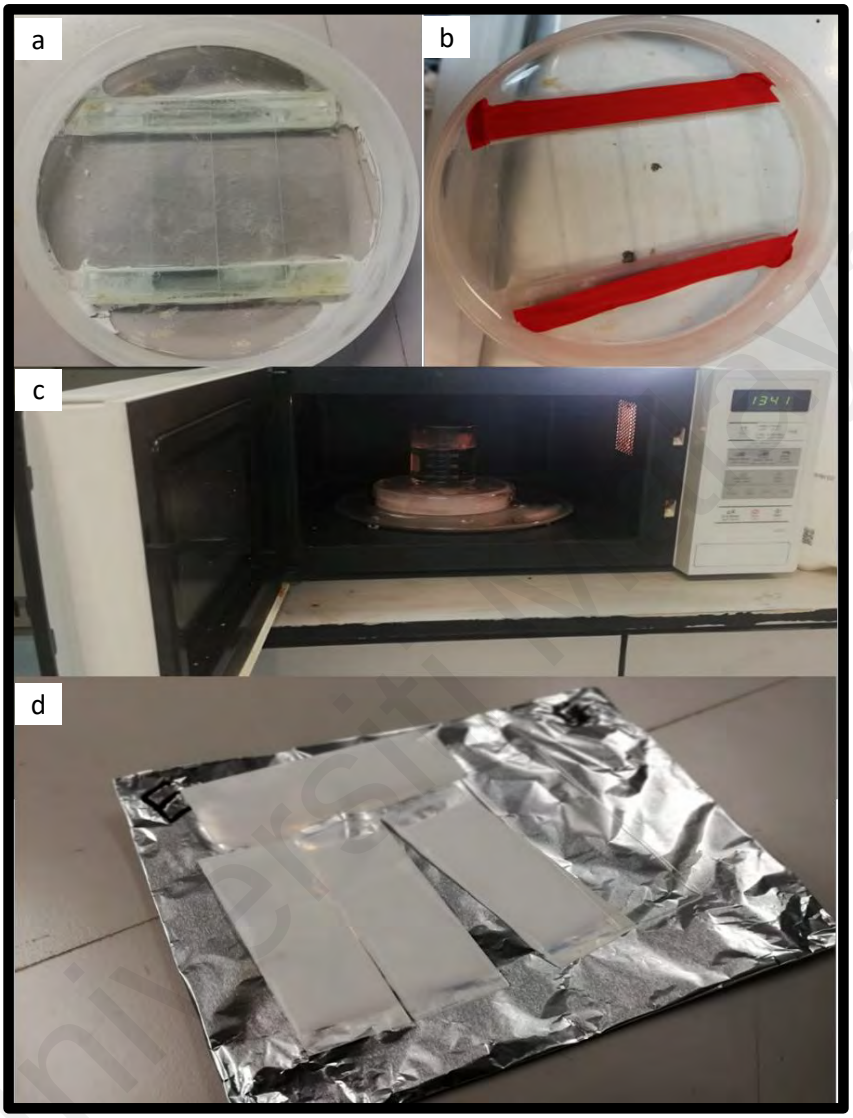

Figure 3.5: Growth Process of ZnO (a) and (b) The seeded slides installed in a glass dish, (c) The glass dish inserted in the microwave, (d) Glass slides after the end of the growth process.

3.2 Characterization

3.2.1 Field Emission Scanning Electron Microscope (FESEM)

The morphologies, diameters, and lengths of GZO nanorods were characterized using a JEOL JSM-7600F field emission scanning electron microscope (FESEM-EDX) working at 20 kV (**Fig. 3.6)**. It is used to analyze and determine the properties of the surfaces of thick or thin samples of the material, to know its shape, and to determine the measures of its external dimensions and its magnification power reaches half a million times. It is very important to know the shape of the material formed on the surface of the glass slides to ensure the formation of nanorods. In addition, the width and length of these nanorods must be measured and compared to ensure the effect of the entry of the element gallium on them. This microscope can determine the elements included in the composition of the sample and their proportions with good accuracy. It works to produce electrons by thermal emission, and this is done by using a heating element usually made of tungsten. An acceleration voltage is applied to it whose value varies between 0.1 - 30 keV, then the electron beam passes through the vacuum microscope column, and a group of electromagnetic lenses along the shaft focuses this beam (Avin, 2019).

The width of the electron beam is controlled by the holes along the column of the microscope, where the scattered and deviated electrons are trapped from the beam path. There are signals from this interaction, the most important of which are the secondary electron emission (SE) signal and the background scattered electron emission (BSE), which are analyzed, processed and shown as images and the X-Ray signal, which is translated into an analytical spectrum (generated). Moreover, using some custom software, you can calculate the dimensions of the sample (Kannan, 2016). **Fig. 3.6** shows the photo of the Field Emission Scanning Electron

Microscope (FESEM). To prepare the samples for the field emission scanning electron microscope, glass slides containing Ga-doped ZnO nanorods were carefully cut with a specialized scalpel. As the dimensions of these samples were 1 × 1 cm. The samples are sprayed with gold or other conductive coating materials.

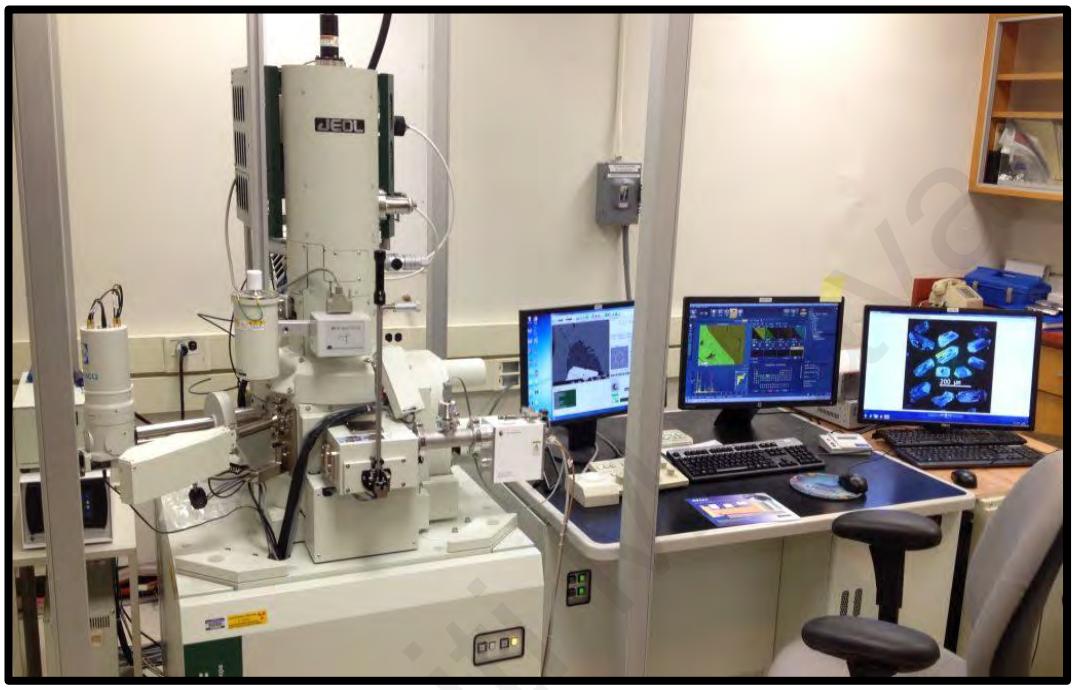

Figure 3.6: JEOL JSM-7600F Field Emission Scanning Electron Microscope (FESEM).

3.2.2 Atomic Force Microscope (AFM)

To examine the outer shape of the nanorods and the root-mean-square (RMS) roughness of the surface, Atomic Force Microscope (AFM) Bruker Dimension Edge with ScanAsyst is used. It is an instrument used to examine surfaces by placing a small probe containing a small thin diamond on the surface of the sample by means of a spring-loaded cantilever. When moving the probe slowly over the sample surface, the force between the surface and the tip is measured, and the probe automatically raised and lowered to maintain this force constant. Surveying the surface in this way allows a computer-aided topographical map to be created (Evan,

2012). The atomic force microscope is very similar to the scanning tunneling microscope (STM) in some ways, although it uses forces rather than electrical signals to examine surfaces. **Fig. 3.7** shows the Atomic Force Microscope (AFM) device and images of nanostructure.

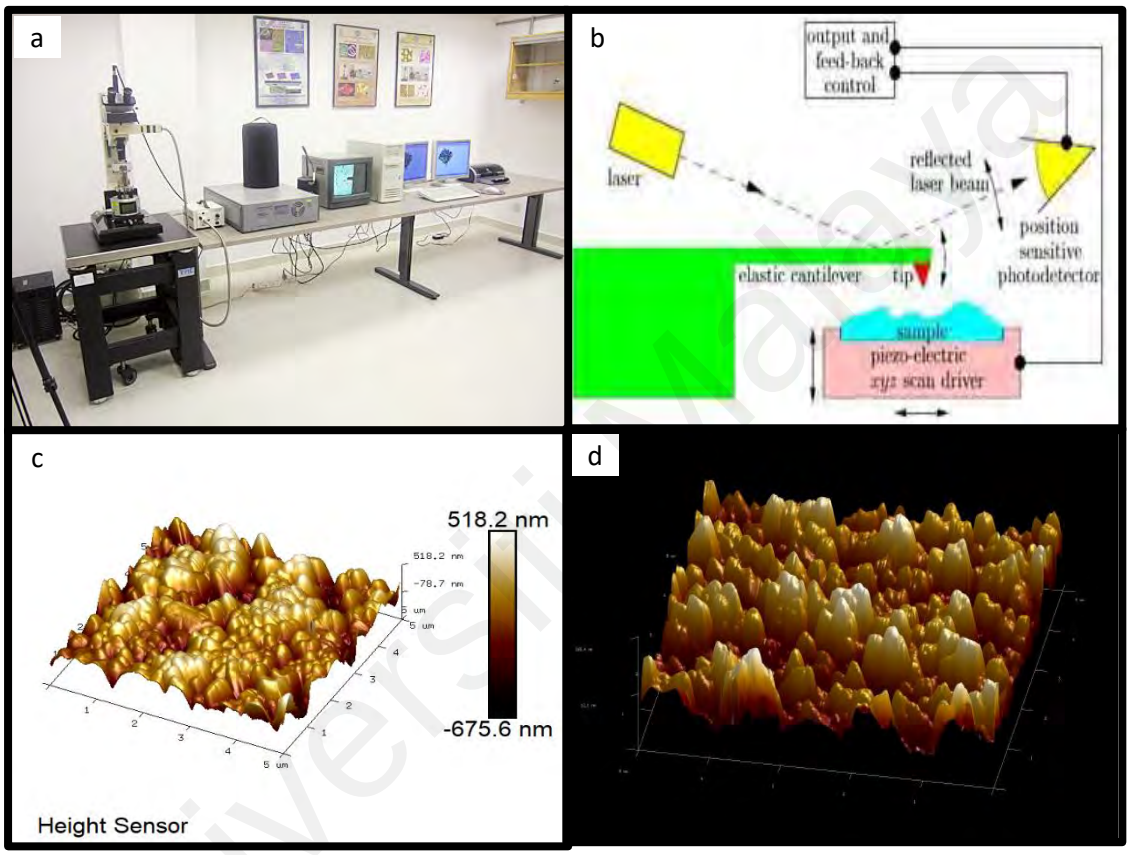

Figure 3.7: (a) Photo of Atomic Force Microscope (AFM), (b) Working mechanism diagram of AFM (Evan, 2012), (c) and (d) AFM 3D images of Nanorods (Sulaiman, 2022).

3.2.3 X-ray Diffraction (XRD)

To confirm the ZnO nanorods crystal growth quality and Ga doping, X-ray diffraction (XRD) measurements were done via Rigaku MiniFlex 600 XRD system with a Cu K_α X-ray source (wavelength ~ 1.54 A^0). It is the effective and non-destructive technique for analyzing crystalline materials, as it provides information about crystal structures, phases and preferred orientation of crystals and the rest of

the structural parameters of materials such as crystallite size of nanomaterials and crystal lattice constants. The wavelengths are scattered at specific angles from a group of crystalline levels of the sample material. The intensity of the scattered rays from the material gives a visualization of the distribution of atoms within the crystal levels of the lattice. The X-ray diffraction chart is considered as a thumbprint for the diagnosis of the substance by comparing the plot of the sample material with the international database such as (ICDD) International Center of Diffraction Data, which gives the structural details of the substance (Banerjee, 2016). This comparison process is performed using X'pert Highscore program and the database Pdf+4 organic, which includes all the standard data for the substances and is updated to 2009 (Speakman, 2019). **Fig. 3.8** shows the X-ray Diffraction (XRD) device and images of nanostructure. Samples were prepared for the XRD device by selecting a completed glass slide for each sample. Then the sample was placed one after another in the place designated for it in the device to take measurements.

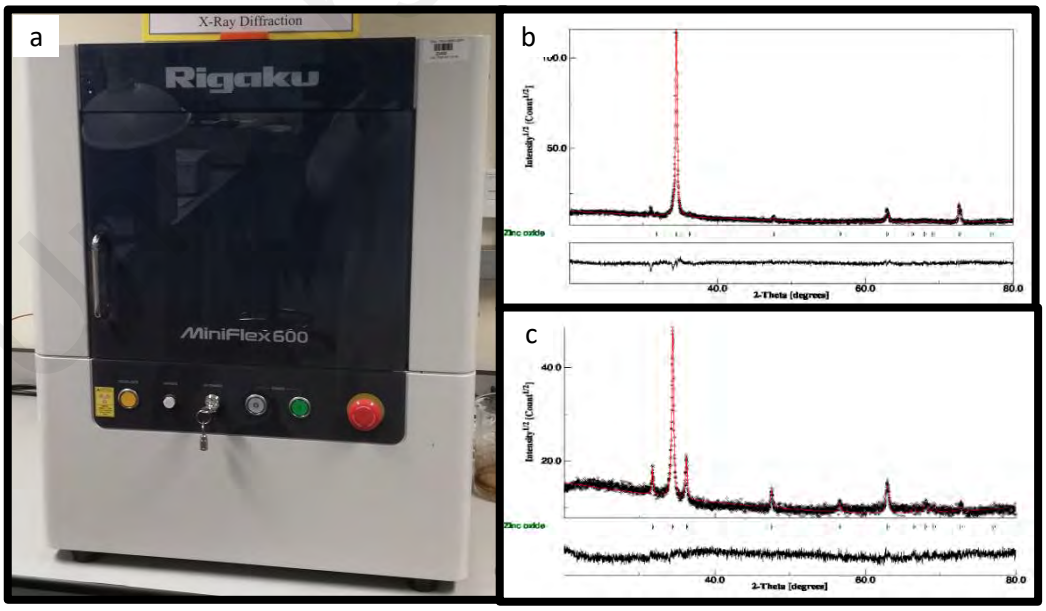

Figure 3.8: (a) Rigaku MiniFlex 600 XRD system, (b) and (c) XRD patterns (Sulaiman, 2022).

3.2.4 Photoluminescence Spectroscopy

Photoluminescence measurements were obtained via a PerkinElmer LS55 fluorescence spectrophotometer using a 325 nm He-Cd laser for excitation. The emission of luminescence occurs when a suitable substance absorbs energy from a source such as ultraviolet light, X-rays, electron beams, chemical reactions, etc. This energy causes the atoms of the material to be excited, transferring them from the ground state to an excited state, and where the excited state is unstable, another transition occurs in which the excited atoms return to the ground level and release energy in the form of light, heat, or both (Sally, 2016).

Excitation involves the electrons of the outer orbit of an atom, and the phenomenon of luminescence depends on the amount of conversion of the excitation energy into light, and there are a few suitable materials that have sufficient luminescence efficiency to be used in practical applications. Photoluminescence technology provides an excellent way to study the luminescence properties of phosphorous materials and has many applications in various fields, some of which are: determining the magnitude of the energy gap, determination of levels of impurities and detection of defects, mechanisms of reconnection and the surface structure and excited planes (Timothy, 2006). **Fig. 3.9** shows the photoluminescence spectroscopy used in this study.

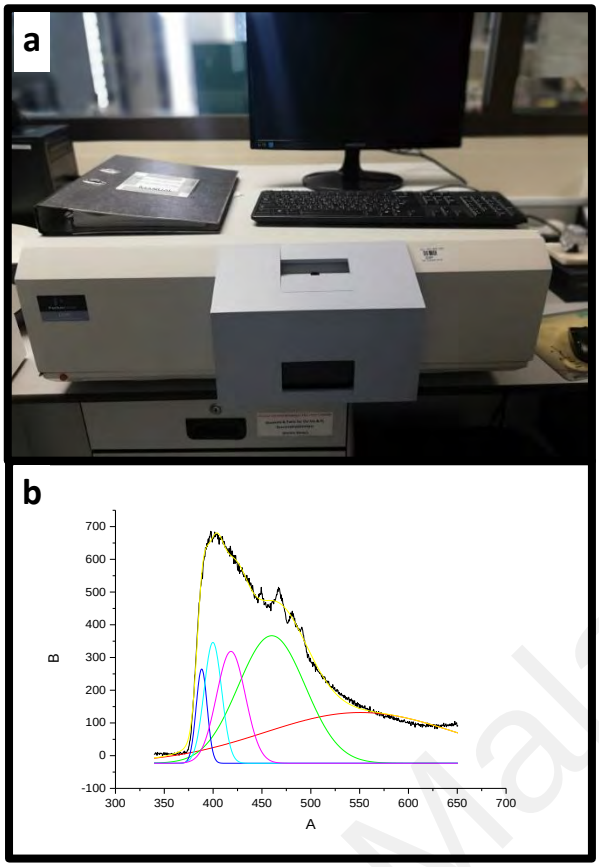

Figure 3.9: (a) PerkinElmer LS55 Photoluminescence Spectroscopy, (b) PL pattern (Sulaiman, 2022).

3.2.5 UV-Vis (UV) Spectroscopy

The optical properties of the samples were analyzed using UV-Visible spectroscopy (Lambda 12 PerkinElmer) at a wavelength of 300 nm – 800 nm. It is one of the types of spectroscopy that depends on the absorption of ultraviolet or visible rays, and it was called by this name because the absorption of rays in these two regions leads to the excitation of electrons in the molecule that absorbs those rays (Regad, 2020). Molecules consist of atoms, each of which consists of a nucleus and electrons revolving around it at specific energy levels. If the molecules absorb a certain energy, the electrons move from a ground state to a higher energy level (excited state). For a light beam to cause an electronic excitation, this beam must be in the visible or ultraviolet range. The frequency of the absorbed beam is related to the

energy with the relationship $E = hf$. In organic molecules, there are three types of electrons. The first type of electrons is shared in a saturated bond, such as the bond between hydrogen and carbon, and carbon in saturated compounds. This bond is called a single bond state. The energy needed to excite bonding electrons is much greater than the energy of ultraviolet rays, so saturated compounds are not absorbed in this area. The second type of electrons are those that share an unsaturated bond. These compounds usually contain double or triple bonds (Caro, 2015). An example of compounds containing three alternating (conjugated) bonds is benzene and alternating hexatriene. The third type of electrons are those that do not share bonds between atoms, and these are called n-free electrons. Saturated organic compounds do not contain *n* electrons because all the electrons in the outer levels of carbon and hydrogen share chemical bonds (Philippidis, 2020). As for organic compounds that contain nitrogen, oxygen, sulfur and halogens, they contain *n* electrons and can absorb visible or ultraviolet rays because these rays can excite *n* electrons.

In conclusion, ultraviolet or visible rays can be absorbed by a compound that contains a nitrogen, oxygen, halogen, or sulfur atom, or contains an unsaturated bond, and the group that contains that is called the absorbing group or the chromophore. **Fig. 3.10** shows the UV-Visible spectroscopy. Samples were prepared for the UV-Vis spectroscopy by selecting a completed glass slide for each sample. Then the sample was placed one after another in the place designated for it in the spectroscopy for measurements. It is necessary to place the sample in the desired absorption range.

Figure 3.10: Lambda 12 PerkinElmer UV-Visible spectroscopy.

3.2.6 Fourier-transform Infrared Spectroscopy (FTIR)

The Fourier transform infrared (FTIR) spectrometer (PerkinElmer, Spectrum One, USA) was used to determine the infrared absorption spectrum of the samples throughout a wavenumber range of 4000 – 400 cm^{-1}, with a signal resolution of 4 cm^{-1} and 40 scans. It was used to confirm the different functional groups that present on pure and doped nanorods samples and may resemble any adsorbed elements on the surface. FTIR spectroscopy is a technology used to obtain infrared absorption or emission of a solid, liquid, or gaseous substance. At the same time, it collects high-resolution spectral data over a wide spectral range. This provides a significant advantage over a scattering spectrometer, which measures intensities over a narrow range of wavelengths simultaneously (S. A. Khan, 2018). Its purpose is to measure the extent to which the sample absorbs light at each wavelength. The most obvious way to do this is with the technique of "dispersion spectroscopy". It's to shine a monochromatic beam of light onto a sample, measure the amount of light absorption, and repeat at each different wavelength. The computer processes the

data using a common algorithm called the Fourier transform (hence the name "Fourier transform spectroscopy"). Raw data is sometimes called "interference" (Berthomieu, 2009). **Fig. 3.11** shows the Fourier-transform Infrared Spectroscopy (FTIR).

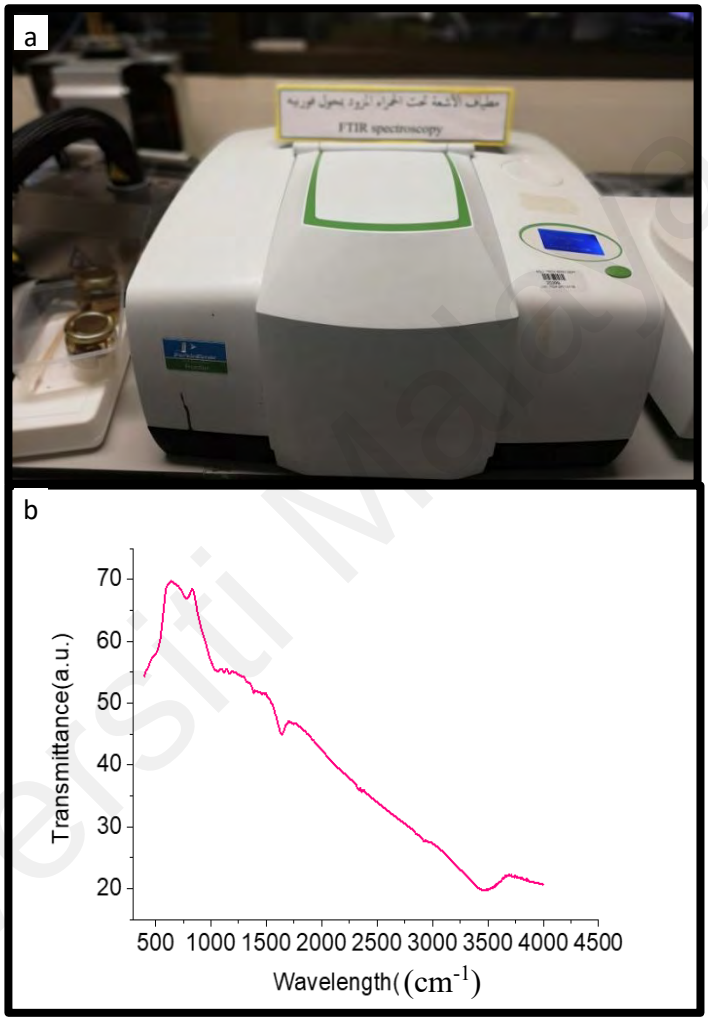

Figure 3.11: (a) Fourier-transform Infrared Spectroscopy (FTIR), (b) FTIR pattern (Sulaiman, 2022).

3.2.7 X-ray Photoelectron Spectroscopy (XPS)

X-ray photoelectron spectroscopy (XPS) is a surface-sensitive quantum spectroscopic technique that measures the elemental composition in parts per thousand groups, the empirical formula, the chemical state and the electronic state

of the elements within a substance (Korin, 2021) (**Fig. 3.12**). XPS spectra are obtained by irradiating the material with a beam of X-rays and at the same time measuring the kinetic energy and number of electrons escaping from the top 0-10 nm of the material being analyzed. XPS requires a high vacuum (P~10 mbar) or ultra-high vacuum (UHV; P<10 mbar), although the current area of development is ambient pressure XPS, where samples are analyzed at pressures of a few tens of millibars. XPS can be used to analyze the surface chemistry of material in its received state, or after some treatment. For example: crushing, cutting, scraping in air or UHV to expose bulk material chemistry or clean ion beams to clean some or all surface contamination (with light ion etching) or to intentionally reveal deep layers of the sample (with more extensive ion etching) in XPS. Deep profiling, exposure to heat to study changes due to heating, exposure to reactive gases or solutions, exposure to ion beam implants, and exposure to ultraviolet light among spectroscopy, refer to those in the X-ray region (Venezia, 2003).

Elemental analysis (suitable for qualitative analysis) determines the atomic number of characteristic X-rays generated by direct electron flow irradiation and checks for fluorescent X-rays (secondary X-rays) generated by applying strong continuous X-rays to a sample of material for fluorescent X-ray analysis (suitable for quantitative analysis). There is also an absorption method in which continuous X-rays are irradiated and analyzed from the X-ray absorption spectrum. It is characterized by the ability to analyze without breaking the sample (Chenakin, 2012).

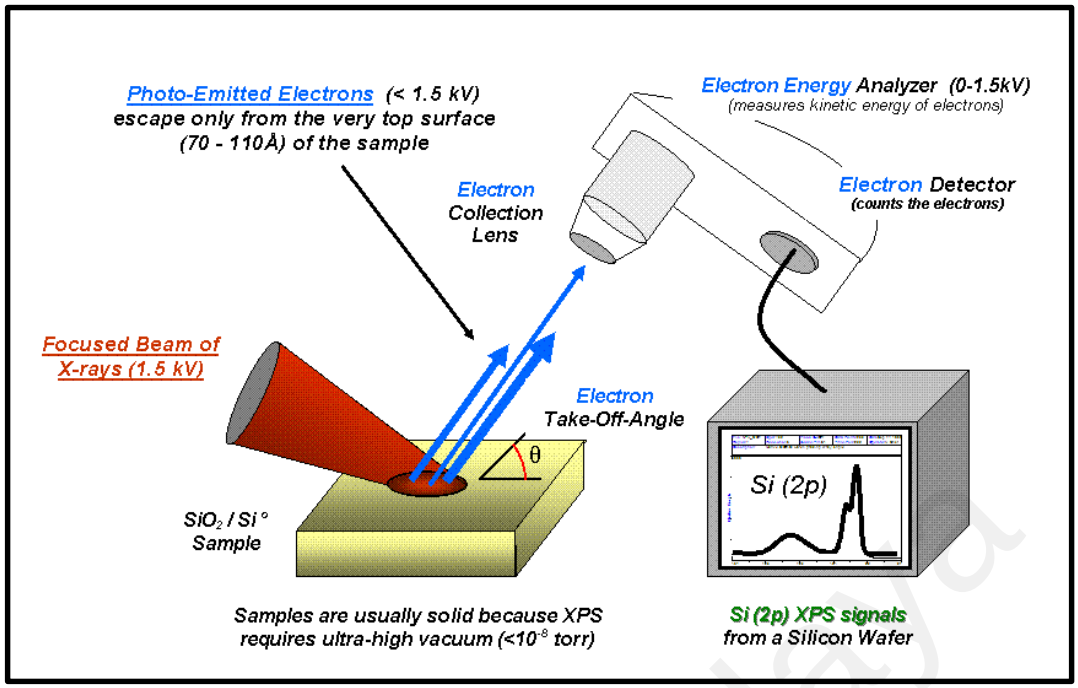

Figure 3.12: Schematic Diagram of X-ray Photoelectron Spectroscopy (XPS) (Korin, 2021).

3.3 Photocatalytic Evaluation

The photocatalytic performance of prepared Ga-doped ZnO samples on a glass substrate under visible and solar light was investigated by monitoring the discoloration of a methylene blue – methylthioninium chloride ($C_{16}H_{18}ClN_3S$, MW 319.85 g/mol) purchased from Sigma Aldrich (Germany). Methylene blue (M.G. AMBIA) solution of 5 ppm is prepared in organic free deionized (DI) water. Generally, the photocatalytic test starts by placing 8 ml of the methylene blue solution (5 ppm) into a 10 ml glass vial. The active glass slide (dimensions of 2.5 cm x 0.9 cm) decorated by ZnO or GZO NRs on the surface was placed vertically in the glass vial and kept under average solar irradiation (1200 W/m^2). A control sample of 5-ppm MB solution without catalyst substrate was used as a control experiment (photolysis test). The photocatalytic process was performed for 2 h, and then decreases in MB concentration were characterized by the UV-Vis spectroscopy (Thermo Scientific™ NanoDrop 2000 and 2000c) instrument. Before

the photocatalytic test, the samples were kept in the dark to maintain the absorption/desorption equilibrium of MB with the ZnO and GZO NRs. In each analysis, 3 ml was taken from the degradation solution tested in the spectrophotometer and returned to the vial for additional degradation time. **Fig 3.13** shows the degradation of the solutions after the photocatalytic test.

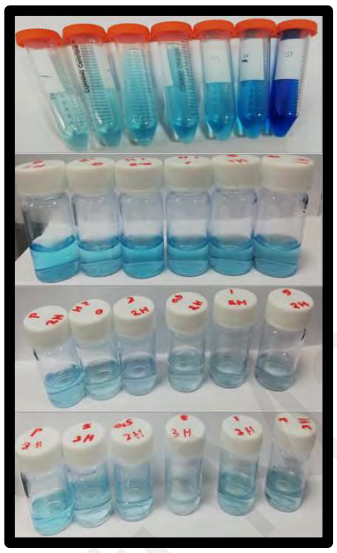

Figure 3.13: Degradation Solutions of Photocatalytic Test

CHAPTER 4: RESULTS & DISCUSSION

4.1 Physical Properties

4.1.1 Hexagonal Wurtzite Ga-doped ZnO

The crystal properties of prepared samples are investigated by XRD analysis. **Fig. 4.1** confirms the well-defined structures of GZO NRs and the Ga doping influence. High-quality GZO with no peaks detected from impurity is produced (B. Al Farsi et al., 2021). The peak positions agreed well with the ZnO (JSPDS. No. 01-080-0075) reference file for all samples. Moreover, the diffraction peaks indexed (100), (002), (101), (103), and (202) with an intense direction along the (002) plane are referred to as a polycrystalline form with a hexagonal wurtzite structure. The intense peak at (002) indicated that the preferred orientation of NRs is perpendicular to the substrate. **Table 4.1** shows the mean crystallite grain size (D) that calculated according to the expansion of the major peak corresponding to the (002) diffraction plane using the Debye–Scherrer formula (Basim Al Farsi et al., 2021).

$$D = \frac{0.9\lambda}{\beta \cos\theta} \tag{4.1}$$

Where, D is the mean crystallite size in nanometer, λ is the X-ray wavelength, β is the FWHM in radians, and θ is Bragg's diffraction angle in degree.

The dislocation density δ is also calculated using the following equation (Muchuweni, 2016a):

$$\delta = \frac{1}{D^2} \tag{4.2}$$

It shows that when the Ga doping percentage is increased, FWHM values at the (002) peak position is increased and then decrease while the mean crystallite sizes (D) are decreased at 1% doping before it starts to increase with the increasing of

doping concentrations. This pattern can be attributed to the incorporation of Ga ions into the ZnO lattice structure, where it has successfully replaced Zn ions in the lattice (Y.-Q. Li, 2010). The lattice parameters *a* and *c* are calculated using the following equation:

$$\frac{1}{d_{hkl}^2} = \frac{4}{3}\left(\frac{h^2 + hk + k^2}{a^2}\right) + \frac{l^2}{c^2} \quad (4.3)$$

Where d_{hkl} is the interplanar spacing obtained from Bragg's law and *h*, *k* and *l* are the Miller indices denoting the plane (Basim Al Farsi et al., 2021). There are no significant changes in lattice parameters of all samples since the un-doped ZnO and GZO nanorods have approximately equal lattice parameters (Gong, 2019). The range of NR crystallite size is between 47.741 and 62.967 nm, in which the smallest crystallite size is recorded by NRs that doped with 1% Ga concentration, while the un-doped NRs possess a larger crystallite size. This phenomenon could be due to the different ionic radius between Zn^{2+} (0.74 and Ga^{3+} (0.61 . Since the ionic radius of Ga^{3+} is smaller than Zn^{2+}, the increase of Ga doping will not increase the crystallite size of NRs. Ga ions are managed to fit into the holes within the ZnO lattice, where the introduction of Ga species during the growth of NRs does not occupy an extra space within the host. Given that the longer and larger NRs length and diameter, respectively, are obtained by 1% Ga-doped ZnO nanorods, the small crystallite size obtained by 1% Ga-doped ZnO nanorods is seen to be correlated. The high nucleation rate can cause the generation of small crystals which lead to a higher growth rate.

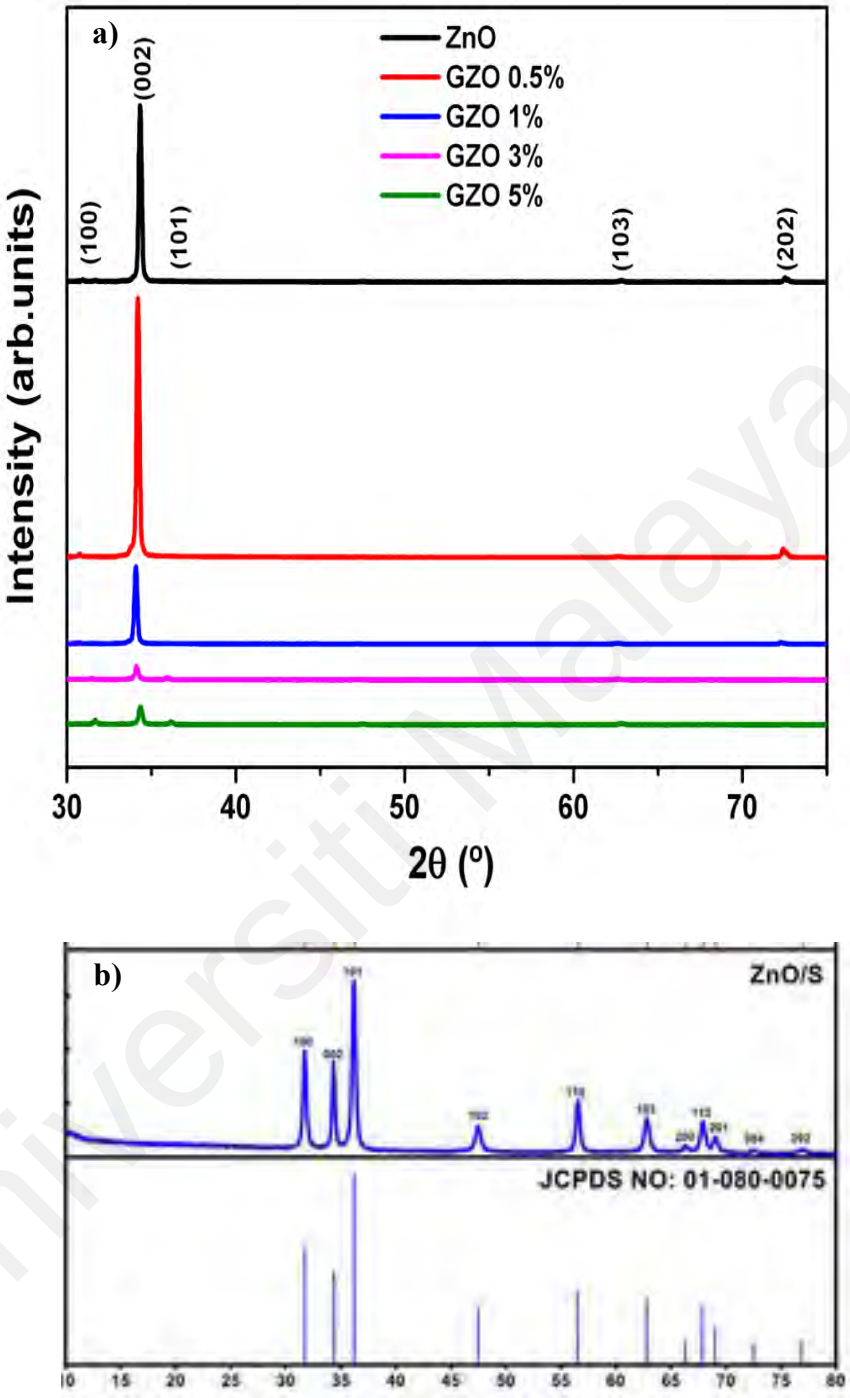

Figure 4.1: a) XRD patterns of the as-prepared samples and b) JCPDS. No. 01-080-0075.

Table 4.1: (002) peak positions, FWHM and mean crystallite size of GZO0, GZO0.5, GZO1, GZO3 and GZO5.

% of Ga doping	Peak position 2θ (°)	FWHM (°)	Crystallite size [nm]	Dislocation density δ [m^{-2}]	Lattice Parameters [Å]
0%	34.319	0.1527	62.967	0.000252	a = 3.248 c = 5.204
0.5%	34.229	0.1622	59.216	0.000282	a = 3.247 c = 5.200
1%	34.319	0.2014	47.741	0.000439	a = 3.249 c = 5.199
3%	34.139	0.1812	52.950	0.000357	a = 3.250 c = 5.202
5%	34.049	0.1683	56.948	0.000308	a = 3.251 c = 5.204

4.1.2 Effect of Ga doping on the Morphology Structure

FESEM and AFM have been conducted to have a profound understanding of the surface morphology of pristine ZnO NRs, and its variation doping percentage of Ga. **Fig. 4.2 (a) – (e)** shows the FESEM images of pristine and Ga-doped ZnO NRs (0, 0.5, 1, 3, 5%), respectively. The images reveal that the variation of nanorods diameters is highly dependent on the percentage of Ga. **Fig. 4.2 (f) – (j)** presents the distribution and average diameters corresponding to its FESEM images. It is observed that there is an increment of NR diameter from the pristine sample until 1% Ga doping, and the diameter starts to reduce at 3% and 5% of Ga doping as shown in **Table 4.2**. All samples show that hexagonal NRs are grown perpendicular to the substrate's surface, but diameters are varied with dopant concentrations. The highest average diameter of 95.4$\pm$0.2 nm is obtained by 1% Ga doping. Without any dopant, NRs are seen to have the smallest average diameter of 63.2$\pm$0.2 nm. The changes in diameter size can be attributed to the incorporation of Ga ions into the ZnO network, which increases the diameter to a certain extent and then reduces the diameter due to the difference in ionic diameter. The addition of Ga above (3%

& 5%) its optimum concentration (1%) into the ZnO lattice will reduce the size of diameter but retains its hexagonal shape. As the objective of this study is to synthesize the NRs, a diameter less than 100 nm is acceptable and potentially be studied for photocatalytic degradation performance. The percentages of Ga concentration (0 – 5%) used in growing the NRs can be said as ideal parameters, however, the performance of a specific application will highly depend on the size of the NRs' diameter. **Fig. 4.3 (a) – (e)** illustrates the FESEM cross-sectional view of pristine and Ga-doped ZnO nanorods of different Ga doping. The corresponding distribution and average of rod length are summarized in **Fig. 4.3(f)–(j),** respectively. The length of the nanorods increases from 0% to 1% of Ga dopant concentration and the length is reduced at 3% and 5% dopant concentration as shown in **Table 4.3**. The length sizes pattern shown from the different Ga dopant concentrations is coherent with the one observed in diameter sizes. For 1% Ga-doped ZnO, both diameter and length have shown a similar pattern, in which the larger size can be reached at this doping before they are reduced with doping is increased to 3% and 5%. This phenomenon can be explained by the behavior of Ga when interacting with the ZnO network.

Table 4.2: Nanorods Diameter of GZO0, GZO0.5, GZO1, GZO3 and GZO5.

% of Ga doping	Diameter [nm]
0	63.2 ± 0.2
0.5	74.1 ± 0. 2
1	95.4 ± 0. 2
3	91.3 ± 0. 2
5	85.2 ± 0. 2

Table 4.3: Nanorods Length of GZO0, GZO0.5, GZO1, GZO3 and GZO5.

% of Ga doping	Length [µm]
0	0.64 ± 0.01
0.5	0.86 ± 0.01
1	2.22 ± 0.02
3	2.15 ± 0.02
5	2.08 ± 0.02

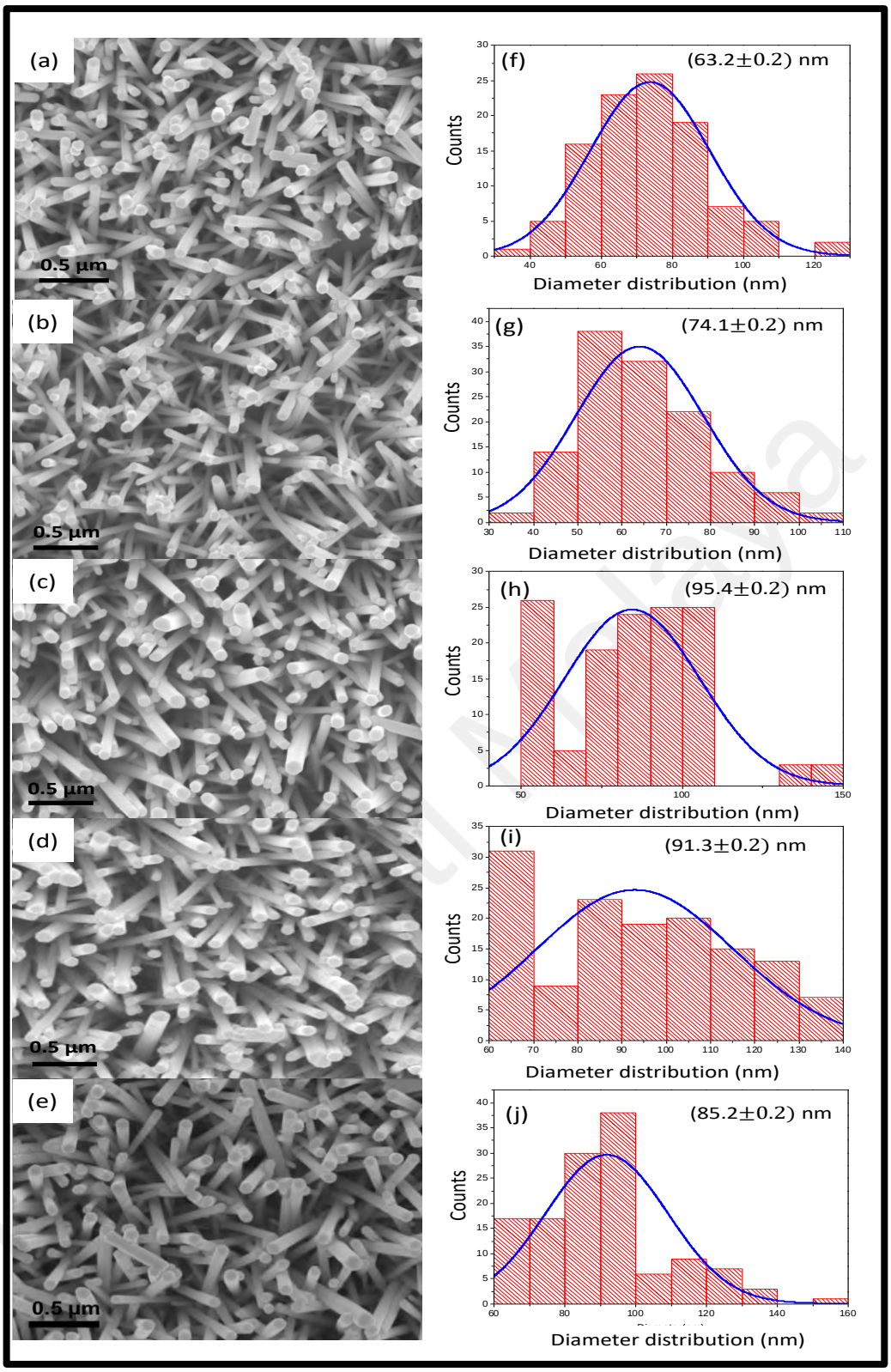

Figure 4.2: FESEM top-view images of (a) pristine, (b) 0.5%, (c) 1.0%, (d) 3.0% & (e) 5.0% and the diameter distribution of (f) pristine, (g) 0.5%, (h) 1.0%, (i) 3.0% & (j) 5.0% of NRs at growth temperature of 550 °C.

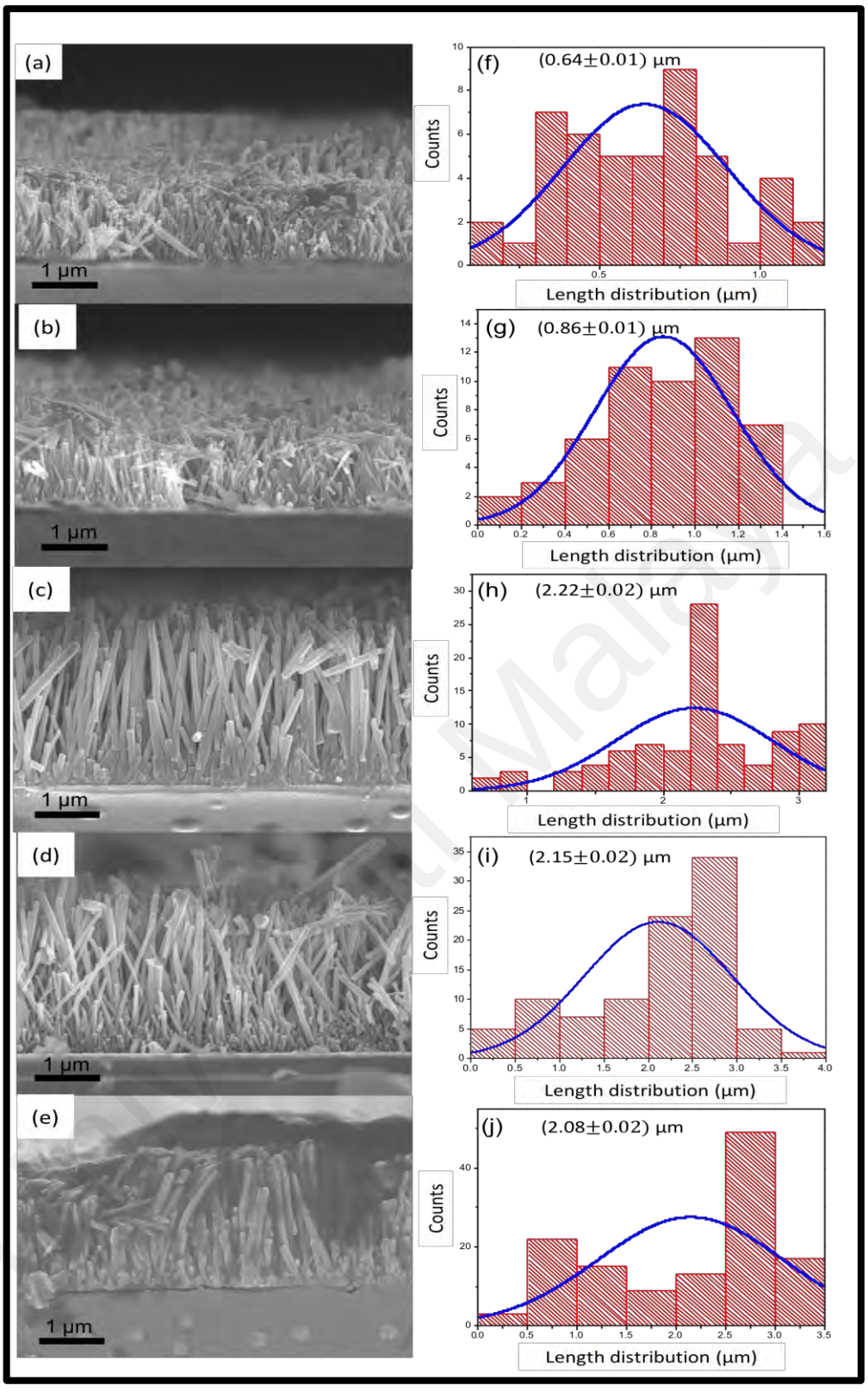

Figure 4.3: FESEM cross-sectional view images of (a) pristine, (b) 0.5%, (c) 1.0%, (d) 3.0% & (e) 5.0% and the length distribution of (f) pristine, (g) 0.5%, (h) 1.0%, (i) 3.0% & (j) 5.0% of NRs at growth temperature of 550 °C.

To support the evident variation in the size and density of nanorods, AFM 3D images are obtained by AFM. **Fig. 4.4 (a) – (e)** shows the AFM 3D images surface topography of GZO0, GZO0.5, GZO1, GZO3, and GZO5, respectively. It can be observed from the figure that topological surface properties obtained from the AFM are in parallel obtained from FESEM, in which the density of nanorods decreases with the increasing Ga doping. The root-mean-square (RMS) surface roughness values of GZO0, GZO0.5, GZO1, GZO3, and GZO5 measured by AFM approximately are 1158.78, 155.86, 83.26, 100.15, and 153.99 nm, respectively as shown in **Table 4.4**. RMS roughness declined with the increase in the Ga doping until 1%, and then it increased with the 3% and 5% doping, which are in accordance with the FESEM images in terms of irregularities. The large RMS means that the sample surface possesses more vacancies for assimilating atoms, nuclei, or particles (Upadhaya & Dhar Purkayastha, 2020). GZO1 recorded the smoother surface with an RMS roughness value of 83.26 nm.

Table 4.4: RMS Roughness Values of GZO0, GZO0.5, GZO1, GZO3 and GZO5.

% of Ga doping	RMS [nm]
0	1158.78
0.5	155.86
1	153.99
3	100.15
5	83.26

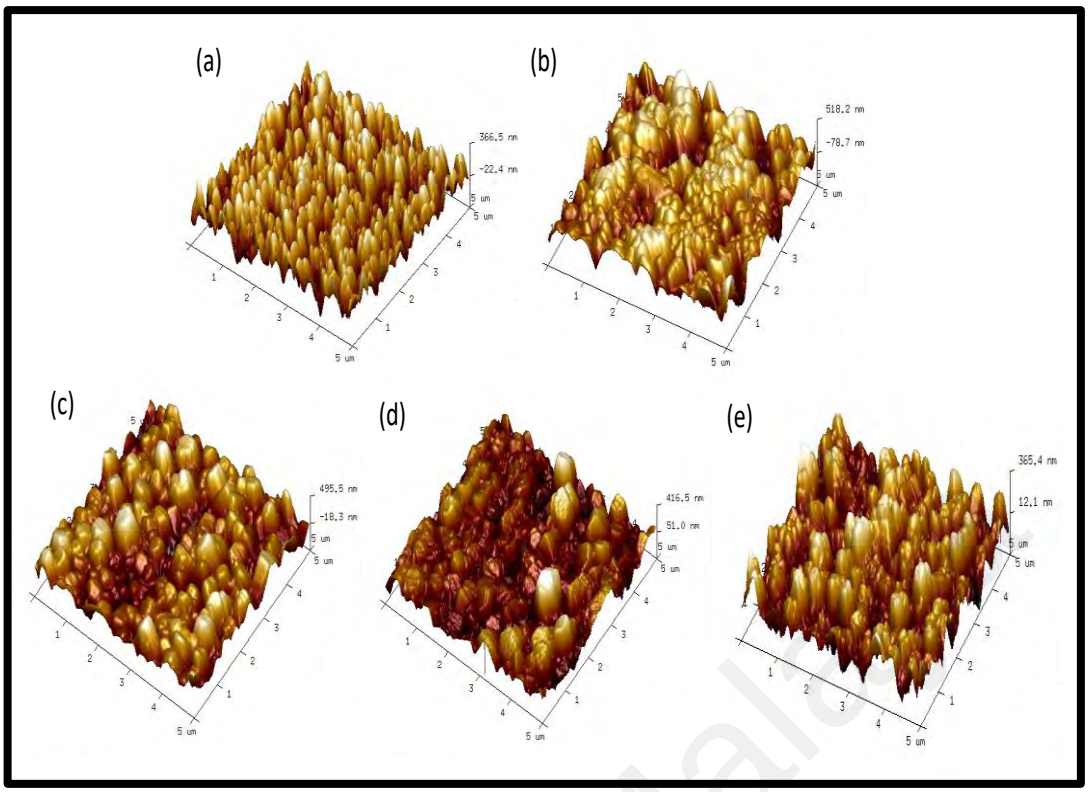

Figure. 4.4: AFM 3D images of (a) GZO0, (b) GZO0.5, (c) GZO1, (d) GZO3 and (e) GZO5.

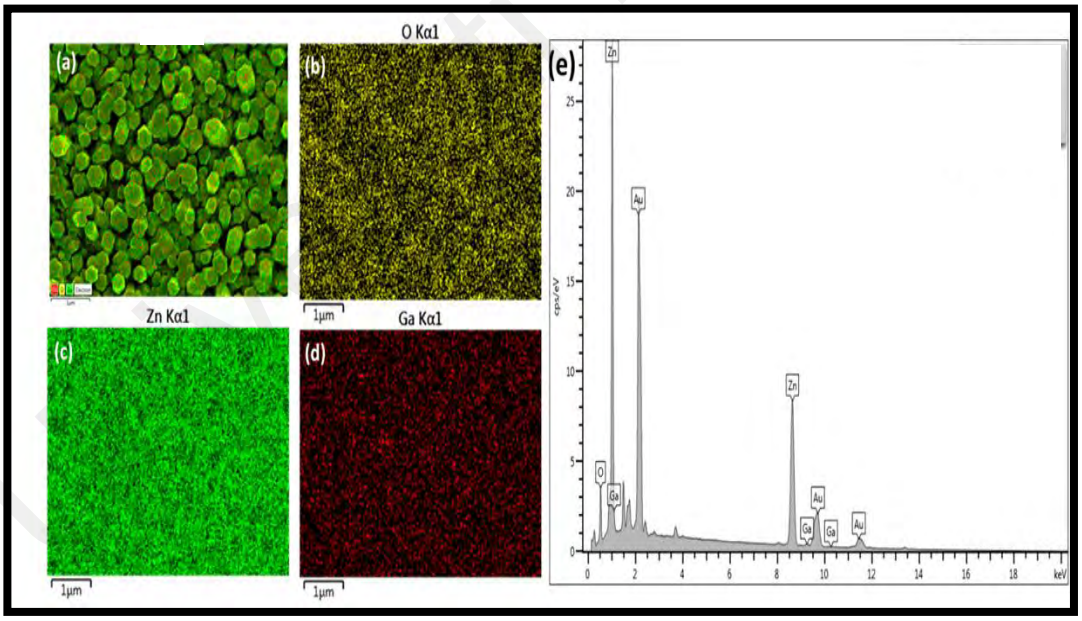

Figure. 4.5: Elemental mapping of GZO1 of (a) all elements distribution, (b) O element, (c) Zn element, (d) Ga element distribution, and (e) Energy-dispersive x-ray spectroscopy (EDS) result of GZO1.

Elemental mapping analysis is performed on the GZO1 sample to show the distribution of major elements within the NRs, as shown in **Fig. 4.5 (a) – (d).** While **Fig. 4.5 (e)** shows the energy-dispersive X-ray spectroscopy (EDX) spectrum of

GZO1. The uniform distribution of Ga, Zn and O elements in the crystal grains is revealed in the maps indicating a homogeneous Ga on NRs' surface along with Zn and O. The detected elements of Zn, O and Ga show the concentration of 86.4%, 12.6% and 1.0%, respectively. Peaks for Au are detected due to the coating used for the sample. Incorporation of Ga into the Zn-O network has occurred which proves well-soluble Ga during the supersaturation phase. Fundamentally, to realize the growth of NRs, supersaturation and nucleation phases are crucial. To reach the supersaturation phase, the concentration of the precursor must exceed the solubility of the system. The growth of Ga-doped ZnO has involved gallium nitrate as a precursor, which has undergone chemical reaction and thermodynamic processes, prior to the nucleation. Ga^{3+} is produced and successfully attached to the ZnO lattice. Based on the EDX, the amount of Ga within the ZnO lattice is relatively low. However, this observation is enough to prove that Ga species have been successfully produced during the chemical reaction process.

Through the images and shapes resulting from the SEM and the AFM, it is seen that the ZnO nanorods are formed, as it appears that there are differences in these nanorods with the difference in the percentage of grafting with gallium. This, in turn, confirms the states of the element gallium in the composition of the ZnO nanorods, and confirms the effect of the proportion of gallium in these nanorods on their shape. Through the images of the SEM and the AFM, the different lengths, and diameters of the nanorods formed by the different percentages of gallium grafting can be seen. Also, a remarkable anomaly appeared in the results of the doping rate of 1% compared to the rest of the percentages.

4.2 Chemical Properties

4.2.1 Surface Chemical Composition Analysis for Ga Doping using XPS Analysis

X-ray Photoelectron Spectroscopy (XPS) is utilized to study the chemical bonding states and identify the relative atomic structure of the chemical elements present in Ga-doped ZnO nanorods. **Fig. 4.6** depicts the typical narrow scan spectra of O1s, Zn 2p and Ga 2p of Ga-doped ZnO nanorods of 0% and 1%. It can be deduced that at 0% Ga-doped ZnO, only Zn and O peaks are observed. **Fig. 4.6a** (i) and (ii) show Gaussian-Lorentzian shape the experimental data of the O element. The O element is deconvoluted into two components located at 530.5 eV and 531.2 eV. The peak located at 530.5 eV is attributed to lattice oxygen atoms O_I, whereas the peak located at 531.2 eV referred to chemisorbed oxygen O_{II}. It is worth noting that, the O_I peak from both samples attributed to the O^{2-} ions in the ZnO crystal lattice, which corresponds to O–M bonds (metal oxides), and the other O_{II} oxygen species peak attributed to chemisorbed or dissociated oxygen on surface hydroxyl, which corresponds to O–H bonds. **Fig. 4.6(b)** portrays the Zn element at 0% and 1% Ga-doped ZnO nanorods sample. The two peaks are located at 1021.8 eV and 1045.0 eV, which may be ascribed to Zn $2p_{3/2}$ and Zn $2p_{1/2}$ electronic states, respectively. While **Fig. 4.6(c)** shows the Ga element present in the 0% and 1% Ga-doped ZnO nanorods sample. It is shown that the Ga peaks only appeared in the 1% Ga-doped ZnO nanorods sample at 1117.9 eV and 1145 eV. These peaks belong to Ga $2p_{3/2}$ and $2p_{1/2}$ electronic states, respectively and are attributed to Ga^{+3} in Ga_2O_3 (Congkang, 2002; Rakhshani, 2009).

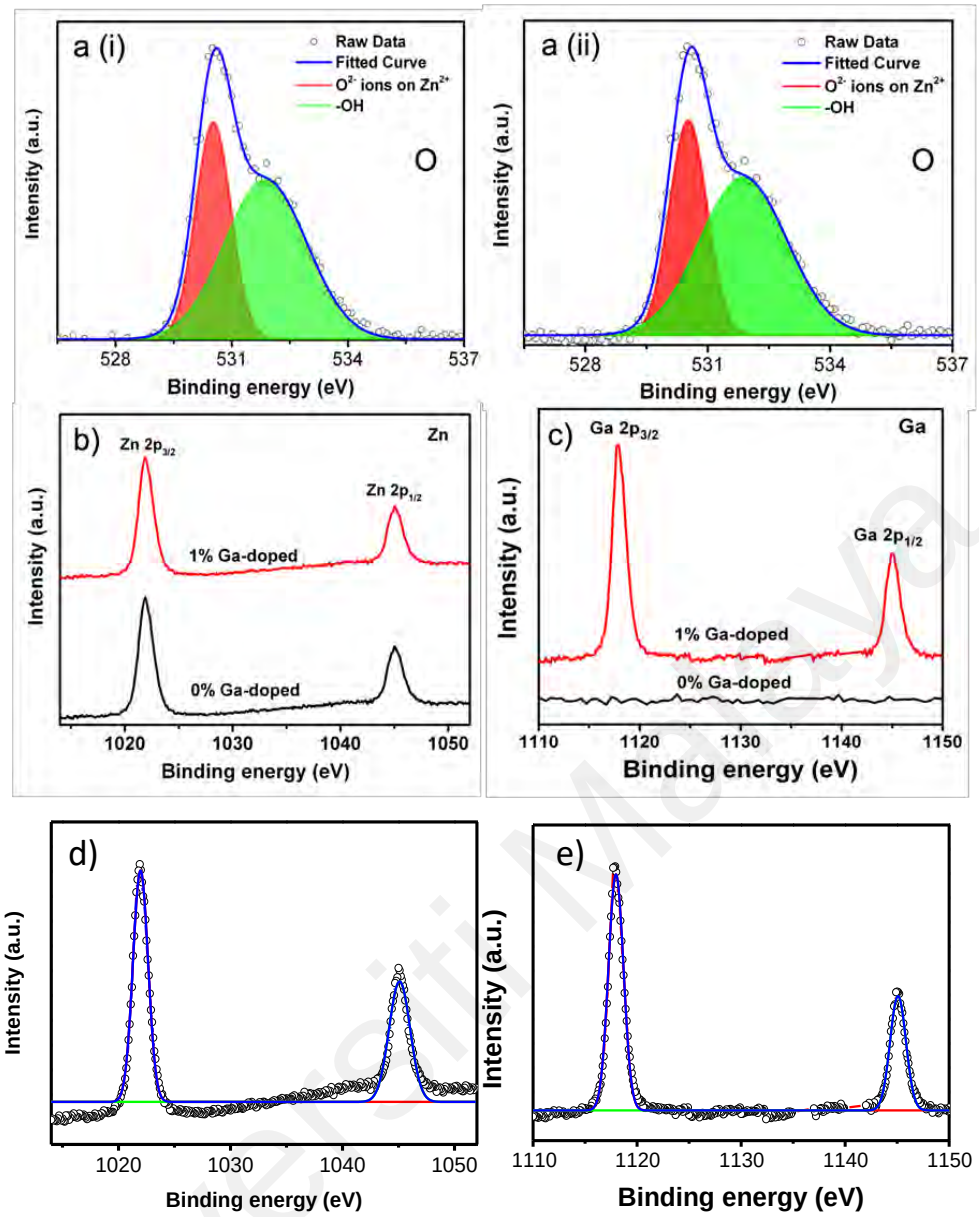

Fig. 4.6: Analyzed XPS spectra, a narrow scan for both 0% and 1%, a) O1s, b) & d) Zn2p and c) & e) Ga2p.

4.2.2 FTIR measurements

The FTIR spectra are essential to confirm different functional groups present on pure and doped nanorods samples (Al-Husaini, Lau, Yusoff, Al-Abri, & Farsi, 2021). The FTIR spectra of Ga-doped ZnO NRs (0%, 0.5%, 1%, 3%, and 5%) are analyzed over 4000–400 cm^{-1} frequency range and measured in ambient air conditions. **Figure 4.7** shows the FTIR spectra of prepared samples. The bands at

450 cm^{-1} are assigned to Zn–O bond vibration mode. The broadband absorption at 545 cm^{-1} that observed for Ga-doped ZnO NRs (0.5%, 1%, 3%, and 5%) is assigned to the asymmetric stretching vibration mode Ga-O bond, which is rise as the percentage of Ga-doping raised. There are also relative intensities of the FTIR spectra in the broadband absorption at 1631 cm^{-1} due to the Zn carboxylate's and symmetrical stretching mode, which appears to be reduced by decreasing the percentage of Ga-doping (Deepashree, 2013). The broadband absorption around 3412–3550 cm^{-1} is ascribed to (-OH) bending vibrations mode of the water molecules absorbed on the Ga-Zn NRs surface, which suggests the existence of Zn-OH radicals incorporated into the Ga-Zn NRs (Ivanova, 2017). These could be remarkable from an electrical point of view because the -OH radicals act as charge carrier traps, which will affect ZnO nanorods electrical properties (Y. Cheng, 2014).

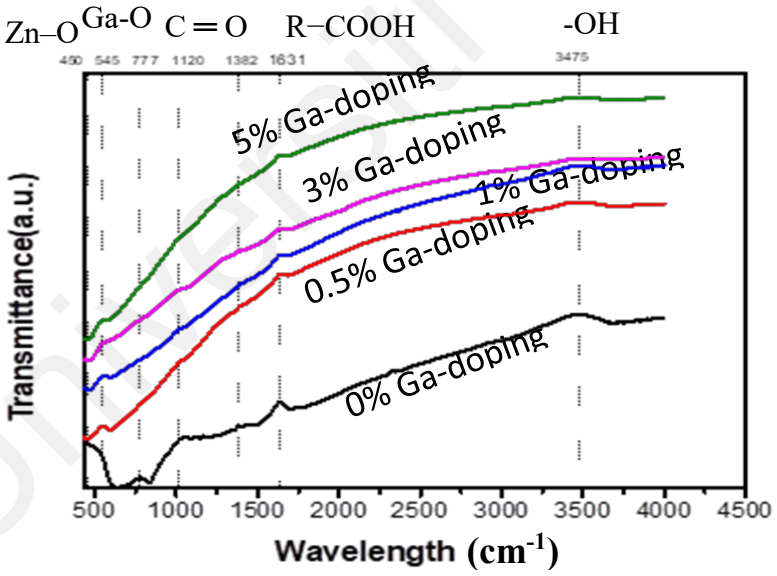

Figure 4.7: FTIR spectrum of Ga-doped nanorods of different doping percentages (0%, 0.5%, 1%, 3% & 5%).

4.3 Optical properties

4.3.1 UV-Vis absorption

Introducing the dopant to the ZnO crystal by changing the Ga-doping percentages will change and improve the optical properties. These optical properties are related to the crystalline structure and electronic properties of the nanorods (Marlene). **Fig. 4.8(a)** shows the UV-Vis absorption spectra of GZO. A significant enhancement in visible light absorbance is observed above the wavelength of 450 nm, especially for GZO1 and GZO5. This red-shift phenomenon of absorption edge can assist in boosting the photocatalytic activity due to the presence of Ga atoms that can change the electronic band structure. The optical energy band gap edge of GZO is presented in **Fig. 4.8(b)**.

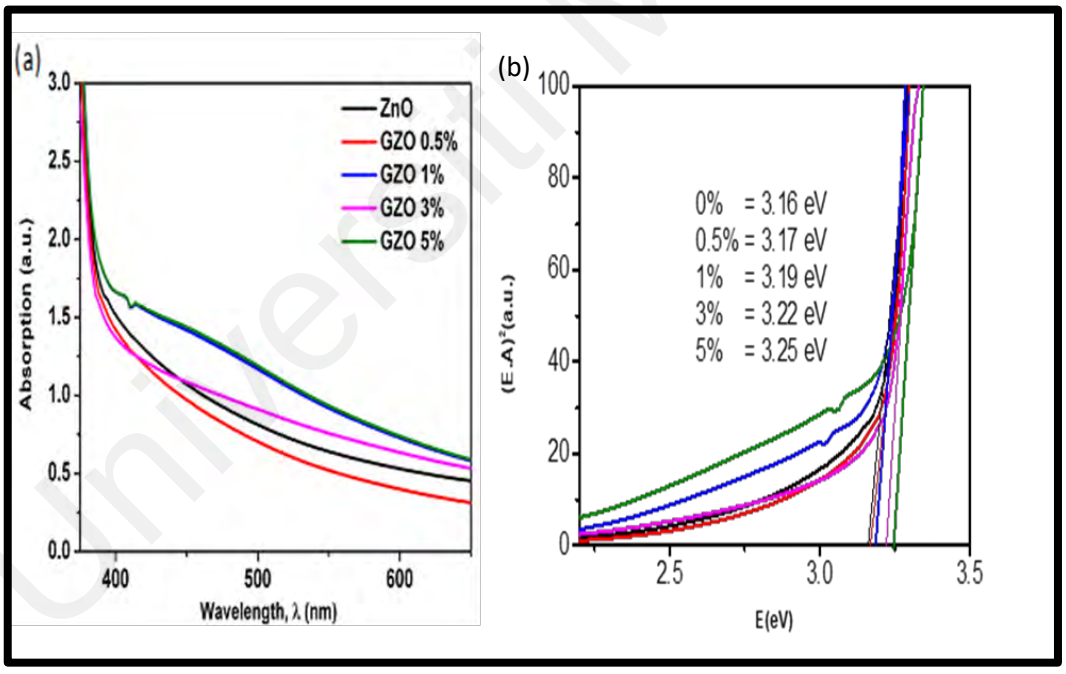

Figure. 4.8: (a) UV-Vis absorption spectra and (b) Tauc's plots of all samples.

The bandgap is calculated from the optical absorption spectra using the Tauc formula:

$$\alpha = \frac{\mathrm{A}\,(\,\mathrm{hv} - Eg\,)^{m}}{\mathrm{hv}} \qquad (4.4)$$

Where α is the absorption coefficient, $h\nu$ is the incident photon energy, E_g is the energy bandgap and m is an exponent factor. m=1/2 is for the direct transition semiconductors and m=2 is for the indirect semiconductors. ZnO is a direct semiconductor, so m = ½ [9, 16]. The determination of direct bandgap energy plots [$(EA)^2$ versus E(Evan)] of the samples are shown in **Fig. 4.8(b)**. Typically, a Tauc's plot shows the quantity (hν) (the photon energy) on the abscissa and the quantity $(\alpha h\nu)^{1/2}$ on the ordinate, where α is the absorption coefficient of the material. Thus, extrapolating this linear region to the abscissa yields the energy of the optical bandgap of the amorphous material. The values of the absorption edge and energy bandgap of GZO are summarized in **Table 4.5**. It is obviously shown that there is a slight variation in the optical bandgap energy values with the dopant concentration. The value of the optical bandgap increases with the increase in the percentage of Ga doping from 3.16 eV to 3.25 eV. This blue shift values may be attributed to the increase in the charge carrier concentration resulting from the difference in the charges of the Ga^{+3} and Zn^{+2} ions which resulted in widen the energy range according to the Burstein–Moss effect (Shtepliuk, 2020).

Table 4.5: The absorption edge and energy band gap of the respective samples.

Name of Sample	Absorption Edge [nm]	Energy Band Gap [eV]
ZnO	389.6	3.16
GZO 0.5%	388.2	3.17
GZO 1%	390.9	3.19
GZO 3%	387.4	3.22
GZO 5%	390.9	3.25

4.3.2 Photoluminescence measurements

Photoluminescence measurements and UV-Vis light diffuse reflection are used to investigate the effect of Ga doping concentrations on the NRs. To obtain the defect emission and the relative change defect due to doping, PL spectra are normalized near the band edge emissions and deconvoluted using the Gaussian function. Emissions are observed wherein both the UV and visible regions. **Fig. 4.9** shows the PL profiles of GZO at room temperature. **Table 4.6** shows the Gaussian peaks of GZO normalized from the PL spectra with all samples possessing identical Gaussian peaks of 393 nm as the band edge emissions (Tiwari, 2015). Significant changes at V_{Zn}, O_i, and V_o emission regions are seen from GZO0.5, GZO1, GZO3 and GZO5. PL emissions in GZO0 have been attributed to different intrinsic defects (V_{Zn}, Zn_i^-, O_i, V_o) and Zn_i^- as an additional defect. The broad emissions of GZO0, GZO0.5, GZO1, GZO3, and GZO5 are observed in the green region (green luminescence), typically attributed to the surface defects in ZnO nanostructures [8, 20]. Green luminescence bands are due to the radial recombination of a photo-generated hole with the electron of singly ionized charged particles in the V_o. These green bands can be seen at around 520 nm for GZO0.5, GZO1, GZO3, and GZO5 and at around 513 nm for GZO0. The zinc vacancy states (V_{Zn}) of GZO0.5, GZO1, GZO3, and GZO5 are recorded at 414 nm and 404 nm recorded by GZO0. The only band at 423 nm is seen from the GZO0, which is related to the zinc interstitial (Z_{ni}) defects (Al-Sabahi, 2016; Basim Al Farsi et al., 2021). The energy levels of intrinsic defects of GZO1 and GZO0 are shown in **Fig. 4.10(a) & (b)**, respectively**.** It shows the clear differences in energy level values between 0% Ga-doped and 1% Ga-doped ZnO NRs. The intrinsic energy defects V_{Zn} and V_0 have lower values in GZO1 than GZO0, while O_i has larger values in GZO1 than GZO0 (Tiwari, 2015).

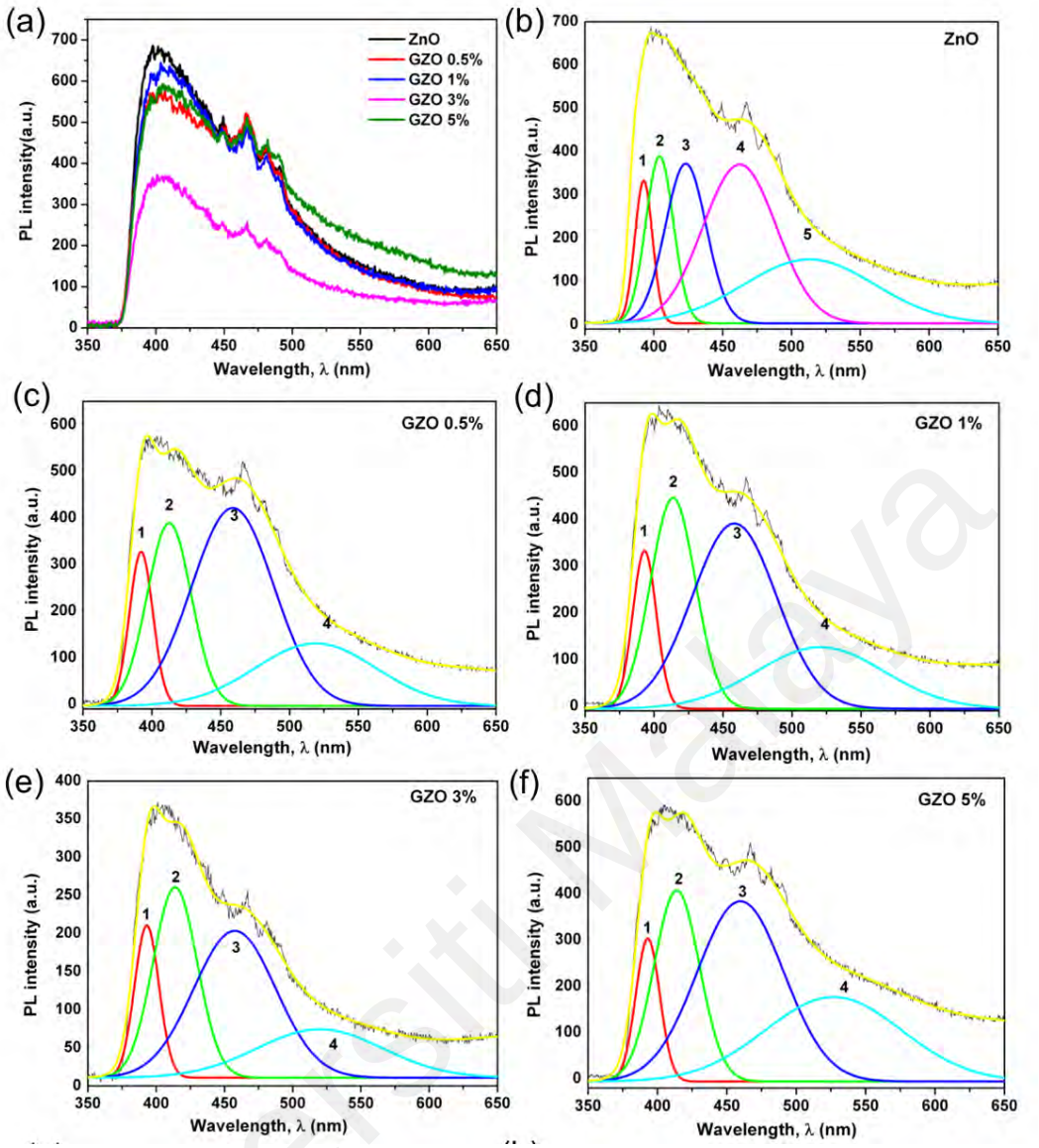

Figure. 4.9: (a) Room-temperature PL spectra of GZO, and de-convoluted PL spectra of (b) GZO0, (c) GZO0.5, (d) GZO1, (e) GZO3 and (f) GZO5.

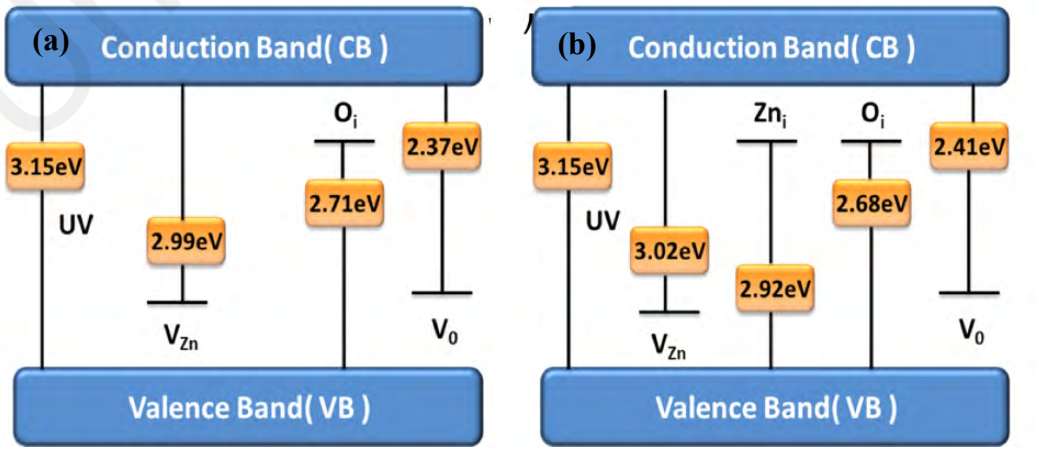

Figure. 4.10: Energy levels of defect states in the band gap of (a) GZO1 and (b) GZO0.

Table 4.6: Gaussian peaks assignments of normalized PL of GZO.

Sample	Peak Position	FWHM	Area (a.u)	Averaged Area (%)	Origin of Emission
ZnO	393	15	5297	7.5	Band edge emission
	404	24	9696	13.6	V_{Zn}
	423	35	13776	19.4	Zn_i^-
	462	63	24624	34.7	O_i
	513	112	17610	24.8	V_0
GZO0.5%	392	20	7052	10.2	Band edge emission
	413	38	15818	22.8	V_{Zn}
	459	70	31743	45.7	O_i
	519	104	14796	21.3	V_0
GZO1%	393	20	7266	10.2	Band edge emission
	414	38	18421	25.8	V_{Zn}
	458	72	30403	42.6	O_i
	520	109	15279	21.4	V_0
GZO3%	393	21	4490	12.3	Band edge emission
	414	38	10139	27.8	V_{Zn}
	458	71	14526	39.8	O_i
	520	109	7348	20.1	V_0
GZO5%	393	20	6724	8.8	Band edge emission
	414	39	17010	22.2	V_{Zn}
	460	73	30481	39.7	O_i
	528	116	22498	29.3	V_0

4.4 Response of NRs during Photocatalytic Process

The photocatalytic performance of GZO samples under solar light has been observed by detecting the concentration of MB. The degradation profile of MB is shown in **Fig. 4.11(a)**, where the initial concentration of MB is 5 ppm and the degradation time is 120 min. The photocatalytic activity of the GZO is estimated by replotting the C/C_o curve vs. time, as shown in **Fig. 4.11(b).** Higher degradation efficiency is observed from the Ga doping samples compared to the un-doped samples. GZO1 shown the highest photocatalytic performance, with more than 80%

degradation achieved within 60 min that caused the destroying of the MB conjugated π system. Improvement in generating the charge carriers of electrons and holes is believed to be the reason for the improved photocatalytic activity of Ga-doped samples as supported by the PL spectra. Moreover, the presence of Ga atoms reduces the bandgap and visible light absorption that leads to better degradation performance.

From the morphological behavior, GZO1 has a larger diameter and length than others. The larger surface area of an individual NR that possesses a larger diameter and length is believed to offer more sites and exposed surfaces for the photocatalytic degradation process to happen over time. A larger number of electrons and holes are predicted to develop on the exposed sites of the NR surface and increase the reaction rate of the photocatalytic. Being the higher aspect ratio of NRs and smallest band gap of 3.17eV, GZO1 has contributed significantly to the photocatalytic activity performances of Ga-doped ZnO NRs. The low crystallite size obtained from XRD analysis leads to a high specific surface area and causes the strongest degradation performance. The ability of degradation performance is measured by the bandgap characteristic of a specific material. Since, GZO1 showed a narrow band gap of 3.17eV, more electrons can jump to the conduction band from the valence band to create the recombination of electron-hole. As more photogenerated carriers are created, more reactions toward oxygen and water to produce free radicals are developed, which is one of the crucial processes in photocatalytic activity.

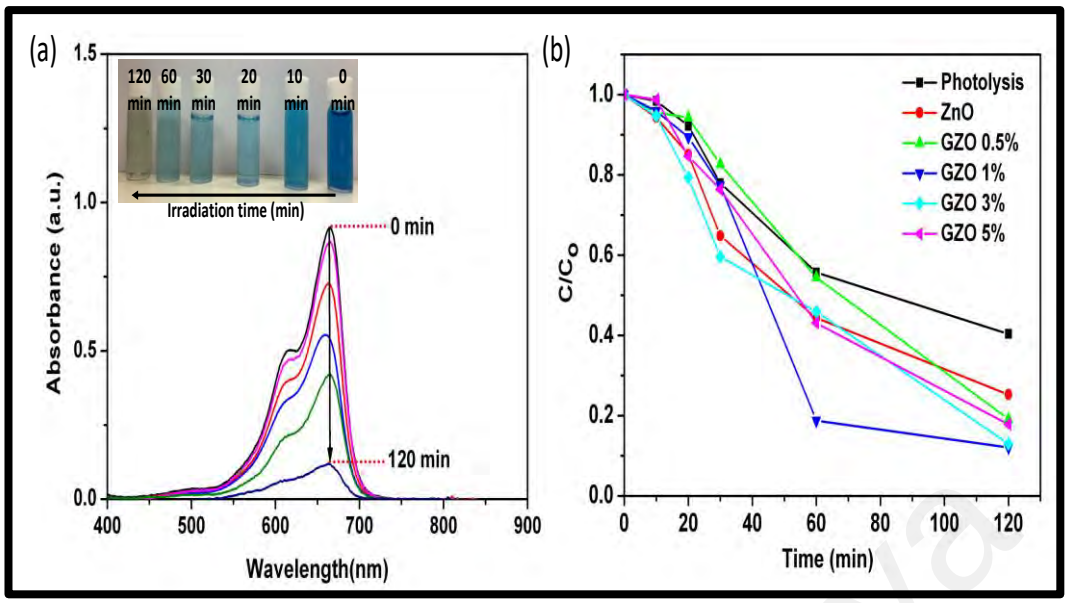

Figure. 4.11: (a) Degradation profile of MB of GZO1 under solar irradiation. (b) Photocatalytic degradation rate within 2 hours of MB.

CHAPTER 5: CONCLUSIONS AND RECOMMENDATIONS

5.1 Conclusions

Rapid synthesis of ZnO and gallium-doped ZnO nanorods have been successfully grown on glass substrates. Different doping levels have been investigated (0, 0.5%, 1%, 3%, and 5% Ga) and characterized by XRD, FESEM, AFM, EDS, XPS, FTIR, UV-Vis spectroscopy, and PL. The efficient degradation of MB in the presence of a prepared sample has been followed systematically. The GZO nanorods are highly transparent with excellent optical transmittance of 85% to 95% in the visible and near IR regions. It was noticed through the XRD results that the crystal size of the ZnO nanorods changed in the various samples used in the experiment, due to the difference in the percentage of gallium doping. In addition, a difference in FWHM was observed for all samples. The results of the 1% sample showed distinct results as it was the lowest in crystal size and the largest in FWHM among all other ratios. It was also shown through the results of infrared absorption that the functional group (OH-) appeared in all samples, which is an important functional group in the photocatalysis properties of the ZnO nanorods. The intensity of the appearance of this functional group differed according to the percentage of gallium doping. Therefore, it appeared significantly in the sample of 1% compared to other samples. Through the results of UV-Vis and PL, it was found that the optical properties and electrical properties of the Ga-doped ZnO nanorods are changed with the change of the doping percentages. The percentages of 1% have a significant change in the absorption of the visible light spectrum, and this in turn made it highly qualified in the photocatalytic activity. The results also showed a noticeable change in the bandgap. This, in turn, changes the electrical properties of the Ga-doped ZnO nanorods. The results of the 1% Ga-doping show that it has low bandgap among the

other percentages. The results of the degradation process of methylene blue dye under solar light also showed a difference in the degradation rate of different doping percentages. 1% Ga-doping has resulted in more degradation of the dye at the given time. Doping at 1% Ga shows more inhabitation for the charge carrier recombination rate with enhancement in photocatalytic activity. This method and result suggested that prepared material can be applied in the applications such as optical and water treatment.

5.2 Future works

It was found through this study that 1% Ga-doping ZnO nanorods are the best percentage, therefore it is worth being included in future work. Studies on the pH characteristics during the preparation of the 1% Ga-doping ZnO nanorods are essential. Apart from the photocatalytic application of Ga-ZnO, it is suggested to include the study of Ga-ZnO nanorods for the UV-Vis light photodetection, to realize the importance of this material as a functional material.

REFERENCES

Abdulrahman, N. A. (2014). *Nanotechnology and chiroptical spectroscopy to characterise optically active chiral metamaterials.* (PhD thesis),

Ahsanulhaq, Q. (2007). Growth of aligned ZnO nanorods and nanopencils on ZnO/Si in aqueous solution: growth mechanism and structural and optical properties. *IOP science, 18*, Article#8.

Al-Husaini, I. S., Lau, W.-J., Yusoff, A. R. M., Al-Abri, M. Z., & Farsi, B. A. A. (2021). Synthesis of functional hydrophilic polyethersulfone-based electrospun nanofibrous membranes for water treatment. *Journal of Environmental Chemical Engineering, 9*(1), Article#11.

Al-Sabahi, J. (2016). Controlled Defects of Zinc Oxide Nanorods for Efficient Visible Light Photocatalytic Degradation of Phenol. *materials, 9*(4), Article#10.

Al Farsi, B., Al Marzouqi, F., Al-Maashani, M., Souier, M. T., Tay Zar Myint, M., & Al-Abri, M. Z. (2021). Rapid microwave-assisted fabrication of Al-doped zinc oxide nanorods on a glass substrate for photocatalytic degradation of phenol under visible light irradiation. Materials Science and Engineering: B, 264, Article#10.

Al Farsi, B., Souier, T. M., Al Marzouqi, F., Al Maashani, M., Bououdina, M., Widatallah, H. M., & Al Abri, M. (2021). Structural and optical properties of visible active photocatalytic Al doped ZnO nanostructured thin films prepared by dip coating. *Optical Materials, 113*, Article#11.

Aldossary, A. N. (2015). *Microwave-Assisted Synthesis and Chemical Modulation of MOF-74(Ni).* (Baccalaureate), University Honors College,

Alexandrov, A. (2020). Al-, Ga-, Mg-, or Li-doped zinc oxide nanoparticles as electron transport layers for quantum dot lightemitting diodes. *Scientific RepoRtS*.

Arakha, M. (2012). *Investigation On The Effect Of Zinc Oxide Nanoparticles In The Aggregation Of Hen Egg Lysozyme.* National Institute of Technology,

Artioli, G. (2007). Crystals and phase transitions in protohistoric glass materials. *Phase Transitions: A Multinational Journal, 81*(2-3), Article#21.

Avin. (2019). Scanning Electron Microscopy (SEM): A Review. *Research Gate*, 10, Article#4.

Banerjee, D. (2016). X-Ray Diffraction (XRD). *IIT Kanpur*, 69, Article#5.

Behera, J. K. (2018). *Synthesis And Characterization Of ZnO Nano-particles.* National Institute Of Technology,

Berthomieu, C. (2009). Fourier transform infrared (FTIR) spectroscopy. *Research Gate, 101*(2-3), Article#15.

Borysiewicz. (2019). ZnO as a Functional Material, a Review. *Crystals, 9*(10), Article#29.

Brix, H. (1995). use of constructed wetlands in water pollution control: historical development, present status, and future perspectives. *pergmond, 30*, Article#15.

Brun, N. (1991). Microstructure of opaque red glass containing copper. *Materials Science Letters*, 3, Article#4.

Buzea, C. (2007). Nanomaterials and nanoparticles: Sources and toxicity. *Biointerphases*, 103, Article#4.

Cai, Z. (2021). Chemical Vapor Deposition Growth and Applications of TwoDimensional Materials and Their Heterostructures. *Chemical Reviews*, 43, Article#4.

Caro, C. A. D. (2015). UV/VIS Spectrophotometry - Fundamentals and Applications. *Research Gate*, 53, Article#6.

Chen. (2011). Tapered aluminum-doped vertical zinc oxide nanorod arrays as light coupling layer for solar energy applications. *Solar Energy Materials and Solar Cells, 95*(6), Article#4.

Chen, B. (2014). Microwave-Assisted Synthesis Of Fluorescent Carbon Nanoparticles. *Texas A&M University*, 122, Article#8.

Chen, X. (2020). Speciation, toxicity mechanism and remediation ways of heavy metals during composting: A novel theoretical microbial remediation method is proposed. *Journal of Environmental Management, 272*, Article#8.

Chenakin, S. (2012). XPS–SIMS Surface Characterization of Aluminovanadate Oxide Catalyst Precursors Co-Precipitated at Different pH: Effect of Calcination. *researchgate, 55*, Article#17.

Cheng, H.-C. (2006). Thin-film transistors with active layers of zinc oxide (ZnO) fabricated by low-temperature chemical bath method. *Science Direct, 498*, Article#4.

Cheng, Y. (2014). Structural, morphological, FTIR and photoluminescence properties of gallium oxide thin films. *Journal of Vacuum Science & Technology B, 32*, Article#5.

Chiu, H.-M. (2015). Fabrication and characterization of well-dispersed plasmonic Pt nanoparticles on Ga-doped ZnO nanopagodas array with enhanced photocatalytic activity. *Applied Catalysis B: Environmental, 163*, Article#11.

Clara. (2020). Aerosol-assisted route to low-E transparent conductive gallium-doped zinc oxide coatings from pre-organized and halogen-free precursor. *Chemical Science, 1039*, Article#11.

Congkang. (2002). A simple and novel route for the preparation of ZnO nanorods. *Solid State Communications, 122*, Article#5.

Conradt. (2011). Catalyst-Free Growth of Zinc Oxide Nanorod Arrays on Sputtered Aluminum-Doped Zinc Oxide for Photovoltaic Applications. *The Journal of Physical Chemistry C, 115*(9), Article#5.

Dai, J. (2006). Microwave-Assisted Extraction And Synthesis Studies And The Scale-up Study With The Aid Of Fdtd Simulation. *Bibliothèque et*, 281, Article#5.

Deepashree. (2013). FTIR Spectroscopic Studies On Cleome Gynandra – Comparative Analysis Of Functional Group Before And After Extraction. *Research Gate, 22*(3-4), Article#8.

Dehghan, M. (2019). Deposition of zinc oxide as an electron transport layer in planar perovskite solar cells by spray and SILAR methods comparable with spin coating. *RSC Advances*, 8, Article#7.

Elshall. (1995). Synthesis And Characterization Of Nanoscale Zinc Oxide Particles .1. Laser Vaporization Condensation Technique. *Nanostructured Materials*.8, Article#6

Evan. (2012). *Atomic Force Microscopy: Lateral-Force Calibration and Force-Curve Analysis.* (Master), Worcester Polytechic Institute.

Farsi, B. A. (2021). Structural and optical properties of visible active photocatalytic Al doped ZnO nanostructured thin films prepared by dip coating. *Optical Materials, 113*, Article#12.

Gawande, M. B. (2014). Microwave-Assisted Chemistry: Synthetic Applications for Rapid Assembly of Nanomaterials and Organics. *American Chemical Society, 47*, Article#11.

Gong, Y. (2019). High acetone sensitive and reversible P- to N-type switching NO2 sensing properties of Pt@Ga-ZnO core-shell nanoparticles. *Sensors and Actuators B: Chemical, 289*, Article#10.

Grewal, A. S. (2013). Microwave assisted synthesis: a green chemistry approach. *Research Gate, 3*(5), Article#9.

Gunkel, G. (2007). Sugar Cane Industry as a Source of Water Pollution – Case Study on the Situation in Ipojuca River, Pernambuco, Brazil. *Water Air Soil Pollut, 180*, Article#9.

Gupta, H. (2019). Defects induced photoluminescence from gallium doped zinc oxide thin films: Influence of doping and energetic ion irradiation. *Physical Chemistry Chemical Physics Please do not adjust margins*, 12, Article#7.

Health, W. (2020). *Progress Report 2001–2011 And Strategic Plan 2012–2020*. Retrieved from Schistosomiasis.

Helen. (2012). Structures of Uncharacterised Polymorphs of Gallium Oxide from Total Neutron Diffraction. *Chemistry_Nanomaterials, 211*, Article#11.

Helland, Å. (2004). Nanoparticles: A Closer Look at the Risks to Human Health and the Environment. *IIIEE, Lund University*, 106, Article#8.

Hong, H.-S. (2010). Humidity sensing characteristics of Ga-doped zinc oxide film grown on a polycrystalline AlN thin film based on a surface acoustic wave. *Sensors and Actuators B: Chemical, 150*, Article#5.

Hsiao, C.-H. (2013). Optical and Structural Properties of Ga-Doped ZnO Nanorods. *Nanoscience and Nanotechnology, 13*, Article#5.

Huang, M. H. (2001). Catalytic Growth of Zinc Oxide Nanowires by Vapor Transport. *ADVANCED MATERIALS, 13*(2), Article#4.

Huang, X.-Y. (2017). Microwave-assisted Liquefaction of Rape Straw for the Production of Bio-oils. *bioresources, 12*(1), Article#14.

Hussein. (2020). Enhancement characterization of the MSM detector based on Mn doped-ZnO NRS synthesized by microwave assisted chemical bath deposition. *Materials Science in Semiconductor Processing, 114*, Article#6.

Ivanova, T. (2017). Structural and morphological characterization of sol-gel ZnO:Ga films: Effect of annealing temperatures. *Thin Solid Films, 17*, Article#32.

Iwantono, I. (2016). Performance of Dye-Sensitized Solar Cell Utilizing Ga-ZnO Nanorods: Effect of Ga Concentration. *International Journal of ELECTROCHEMICAL SCIENCE, 11*, Article#8.

Jimenez-Cadena. (2010). Synthesis Of Different Zno Nanostructures By Modified Pvd Process And Potential Use For Dye-Sensitized Solar Cells. *Materials Chemistry And Physics, 124*(1), Article#4.

Jin, S. (2018). *Manipulation of electronic band structure by doping colloidal gallium oxide nanocrystals and its impact on photocatalysis.* (Master), University of Waterloo,

Johnson-McDaniel, D. (2013). Nanoscience of an ancient pigment. *American Chemical Society, 135*, Article#3.

Jorge. (2012). Zinc oxide nanostructures: from growth to application. *Springer Science, 48*, Article#13.

Kamaruddin, S. A. (2010). Zinc oxide films prepared by sol–gel spin coating technique. *Springer-Verlag, 104*, Article#6.

Kannan, D. M. (2016). Scanning Electron Microscopy: Principle, Components and Applications. In *A Textbook on Fundamentals and Applications of Nanotechnology* (pp. 80-92).

Karabulut, A. (2021). Zinc oxide based 3-components semiconductor oxide photodiodes by dynamic spin coating method. *Materials Science in Semiconductor Processing, 134*, Article#11.

Kazi. (2020). Microwave assisted synthesis of zinc oxide (ZnO) nanoparticles in a noble approach: utilization for antibacterial and photocatalytic activity. *Springer Nature Switzerland, 955*(2), Article#14.

Khan, I. (2017). Nanoparticles: Properties, Applications and Toxicities. *Arabian Journal of Chemistry, 17*, Article#70.

Khan, S. A. (2018). Fourier Transform Infrared Spectroscopy: Fundamentals and Application in Functional Groups and Nanomaterials Characterization. *Research Gate, 82*, Article#29.

Khorshidi, Z. G. (2021). Photocatalytic Analysis of a Hydrophilic Acrylic Coating/ Zinc Oxide Nanocomposite on Glass Substrate. *Polymer-Plastics Technology and Materials, 60*(11), Article#14.

Koc, M. u. M. (2018). Electrical Characterization of Solar Sensitive Zinc Oxide Doped-Amorphous Carbon Photodiode. *Optik Optics, 18*, Article#29.

Korin, E. (2021). Surface Analysis of Nanocomplexes by X-ray Photoelectron Spectroscopy (XPS). *ACS Biomater, 6*(3), Article#8.

Kreuter, J. o. (2006). Nanoparticles—a historical perspective. *International Journal of Pharmaceutics, 331*(1), Article#10.

Kumar, M. (2010). *Zinc Oxide Nanostructures Synthesized by Oxidization of Zinc.* (Bachelor of Technology), National Institute of Technology,

Kumar, S. (2013). Structure, Morphology, and Optical Properties of Amorphous and Nanocrystalline Gallium Oxide Thin Films. *The Journal of Physical Chemistry C, 117*, Article#7.

Kunduru, K. R. (2012). Nanotechnology For Water Purification: Applications Of Nanotechnology Methods In Wastewater Treatment. *he Hebrew University of Jerusalem, 71*, Article#42.

Lee, J.-H. (2012). Synthesis of Ga-Doped ZnO Nanorods Using an Aqueous Solution Method for a Piezoelectric Nanogenerator. *Nanoscience and Nanotechnology, 12*, Article#6.

Leong, K. H. (2018). Light Driven Nanomaterials for Removal of Agricultural Toxins. *researchgate, 23*, Article#19.

Li, X. (2016). Ga doped ZnO photonic crystals with enhanced photocatalytic activity and its reaction mechanism. *Applied Catalysis B: Environmental, 195*, Article#10.

Li, Y.-Q. (2010). Preparation and electrical properties of Ga-doped ZnO nanoparticles by a polymer pyrolysis method. *Materials Letters, 64*, Article#3.

Liu, X. (2013). Review on the Synthesis and Applications of Fe3O4 Nanomaterials. *Nanomaterials, 10*, Article#8.

Luo, J. (2021). Improved Photovoltaic Characteristics of Inverted Polymer Solar Cells With Indium-Doped ZnO at Low-Temperature Annealing as Electron-Transport Layer. *IEEE Journal Of Photovoltaics, 11*(2), Article#5.

M.G. AMBIA. (1994). The effects of deposition variables on the spray pyrolysis of ZnO thin film. *Mateeerials Science, 29*, Article#6.

Mabrouk, M. (2021). Nanomaterials for Biomedical Applications: Production, Characterisations, Recent Trends and Difficulties. *molecules, 26*, Article#27.

Majdi. (2021). Enhanced Photocatalytic Removal of Cyanotoxins by Al-Doped ZnO Nanoparticles with Visible-LED Irradiation. *toxins, 13*, Article#14.

Majeed, S. (2017). Principles and Advantages of Microwave-Assisted Methods for the Synthesis of Nanomaterials for Water Purification. *Research Gate, 36*, Article#24.

Malsch, I. (2005). *Benefits, Risks, Ethical, Legal and Social Aspects of Nanotechnology*. Retrieved from

Mamat. (2011). Fabrication of ultraviolet photoconductive sensor using a novel aluminium-doped zinc oxide nanorod–nanoflake network thin film prepared via ultrasonic-assisted sol–gel and immersion methods. *Sensors and Actuators A: Physical, 171*(2), Article#241-247.

Manuja, A. (2020). Microwave assisted fast fabrication of zinc/iron oxides based polymeric nanocomposites and evaluation on equine fibroblasts. *International Journal of Biological Macromolecules*, 11, Article#7.

Marlene. (2019). Photocatalytic and Antimicrobial Properties of Ga Doped and Ag Doped ZnO Nanorods for Water Treatment. *Catalysts, 9*(2), Article#6.

Maurya, M. R. (2019). Wide spectral photoresponse of template assisted out of plane grown ZnO/NiO composite nanowire photodetector. *Nanotechnology*, 8, Article#9.

Mie. (1908). Annalen Der Physik. *Greifswald, 52*, Article#69.

Mindy. (1998). Nanostructured Materials: An Overview and Commercial Analysis. *Emerging Technologies, 7*, Article#2.

Mohapatra, D. R. K. (2020). Nanomaterials. *Chemistry_Nanomaterials, 6*, Article#16.

Morris, J. (2007). *Nanotechnology White Paper*. Retrieved from

Muchuweni, E. (2016a). Effect of gallium doping on the structural, optical and electrical properties of zinc oxide thin films prepared by spray pyrolysis. *Ceramics International*, 5, Article#7.

Muchuweni, E. (2016b). Effect of gallium doping on the structural, optical and electrical properties of zinc oxide thin films prepared by spray pyrolysis. *Ceramics International, 42*, Article#5.

Murali, A. (2018). Enhanced Photocatalytic Activity and Photocurrent Properties of PlasmaSynthesized Indium-Doped Zinc Oxide (IZO) nanopowder. *Elsevier, 34*, Article#29.

Norton, D. P. (2004). ZnO: growth, doping & processing. *materialstoday, 7*(6), Article#7.

Nouailhat, A. (2006). An Introduction to Nanoscience and Nanotechnology. *Library of Congress Cataloging-in-Publication Data, 176*(8), Article#229.

Park, S. (2018). Photocurrent Characteristics of Zinc-Oxide Films Prepared by Using Sputtering and Spin-Coating Methods. *Journal of the Korean Physical Society, 73*(9), Article#5.

Philippidis, A. (2020). Application of Ultraviolet-Visible Absorption Spectroscopy with Machine Learning Techniques for the Classification of Cretan Wines. *Foods, 10*(1), Article#12.

ponja, S. D. (2020). Highly conductive and transparent gallium doped zinc oxide thin films via chemical vapor deposition. *Scientific RepoRtS, 61*(1), Article#7.

Rajaram, T. (2008). Water pollution by industrial effluents in India: Discharge scenarios and case for participatory ecosystem specific local regulation. *Science Direct, 40*, Article#14.

Rajendra. (2013). Fabrication of nanocomposite photocatalysts from zinc oxide nanostructures and reduced graphene oxide. *Current Applied Physics, 13*(2), Article#8.

Rakhshani, A. E. (2009). Structure, composition and optical properties of ZnO:Ga films electrodeposited on flexible substrates. *Applied Physics A, 97*, Article#6.

Ramesh. (2021). Enhanced optoelectronic properties of Ti-doped ZnO nanorods for photodetector applications. *Ceramics International, 47*(17), Article#8.

Rasouli, F. (2018). Fabrication of silver nanoparticles decorated zinc oxide nanotubes by electrodeposition technique for photoelectrochemical water splitting. *Materials Science in Semiconductor Processing, 93*, Article#8.

Regad. (2020). Basic UV-Vis Theory, Concepts and Applications. *Thermo Spectronic, 78*(3), Article#28.

Runowski, M. (2014). Nanotechnology - nanomaterials, nanoparticles and multifunctional core/shell type nanostructures. *Research Gate, 68*(9), Article#6.

S.Hingorani. (1993). Microemulsion Mediated Synthesis Of Zinc-Oxide Nanoparticles For Varistor Studies. *Research Bulletin, 28*, Article#8.

Saini, S. (2019). Porosity-tuned thermal conductivity in thermoelectric Al-doped ZnO thin films grown by mist-chemical vapor deposition. *Thin Solid Films, 19*, Article#22.

Sally. (2016). An Introduction To Photoluminescence Spectroscopy For Diamond And Its Applications In Gemology. *Feature Rticles, 52*(1), Article#16.

Samsung. (2011). - Asia's new model company. *London, United Kingdom*.

Santibenchakul. (2018). Ga-doped ZnO nanoparticles synthesized by sonochemical-assisted process. *Materials Today: Proceedings, 5*(6), Article#13865-13869.

Sathish, P. (2021). Combustion synthesis, characterization and antibacterial properties of pristine ZnO and Ga doped ZnO nanoparticles. *Ceramics International*.

Schaming, D. (2015). Nanotechnology: from the ancient time to nowadays. *Springer Science, 63*(1), Article#19.

Schwarzenbach. (2012). Global Water Pollution and Human Health. *Annual Review Of Environment And Resources, 35*, Article#32.

Schwarzenbach, R. e. P. (2012). Global Water Pollution and Human Health. *annual reviews*, 32, Article#9.

Shtepliuk, I. (2020). Excitonic emission in heavily Ga-doped zinc oxide films grown on GaN. *Journal of Luminescence, 223*, Article#10.

Sikam, P. (2019). The study of structural, morphological and optical properties of (Al, Ga)-doped ZnO: DFT and experimental approaches. *Applied Surface Science, 19*, Article#41.

Speakman, S. A. (2019). Basics of X-Ray Powder Diffraction. *Center for Materials Science and Engineering at MIT, 617*, Article#97.

Stepanov. (2016). Gallium Oxide: Properties And Applications - a Review. *Advanced Materials, 44*, Article#24.

Sulaiman. (2022). Ga-doped ZnO nanorods: The photocatalytic performance of methylene blue under solar irradiation. *Optical Materials, 126*, Article#10.

Tahir, M. B. (2020). Role of Nanotechnology in Photocatalysis. *Encyclopedia of Smart Materials, 12*, Article#12.

Tian, T. (2018). Hydrogen Generation from Eosin Y-sensitized Pt/ZnO under Solar Light Irradiation. *Electronic Thesis and Dissertation Repository, 45*(2), Article#94.

Timothy. (2006). Photoluminescence in Analysis of Surfaces and Interfaces. *Encyclopedia of Analytical Chemistry, 26*(2), Article#23.

Tiwari, N. (2015). Structural, optical, and photoluminescence study of ZnO/IGZO thin film for thin film transistor application. *Materials Letters, 151*, Article#4.

Trotta, F. (2013). Nanomaterials: Classification and Properties. *Nanosponges, 52*, Article#26.

Upadhaya, D., & Dhar Purkayastha, D. (2020). Enhanced wettability and photocatalytic activity of seed layer assisted one dimensional ZnO nanorods synthesized by hydrothermal method. *Ceramics International, 46*(10), Article#15831-15839.

Urper, O. (2020). Effect of Al concentration on optical parameters of ZnO thin film derived by Sol-Gel dip coating technique. *Materials Letters, 274*, Article#4.

Vance, M. E. (2015). Nanotechnology in the real world: Redeveloping the nanomaterial consumer products inventory. *journal of nanotechnology, 6*, Article#12.

Venezia, A. M. (2003). X-ray photoelectron spectroscopy (XPS) for catalysts characterization. *Catalysis Today, 77*, Article#12.

Vivekanandan, A. K. (2020). Size-controllable zinc oxide nanowires fabricated via the combination of die-casting and oxidation process. *Journal of Alloys and Compounds, 861*, Article#8.

Wahab, R. (2011). Fabrication, characterization and growth mechanism of heterostructured zinc oxide nanostructures via solution method. *Current Applied Physics, 11*, Article#7.

Wan, Q. (2013). Fabrication and ethanol sensing characteristics of ZnO nanowire gas sensors. *APPlied Physics Letters, 84*, Article#4.

Wang, Y. (2021). Surface Plasmon Resonance from Gallium-Doped Zinc Oxide Nanoparticles and Their Electromagnetic Enhancement Contribution to Surface-Enhanced Raman Scattering. *Applied Materials, 13*, Article#8.

Xingjian. (2018). Petroleum Hydrocarbon-Degrading Bacteria for the Remediation of Oil Pollution Under Aerobic Conditions: A Perspective Analysis. *Frontiers in Microbiology, 195*, Article#11.

Yang. (2020). Enhanced Acetone Sensing Properties of Pt@Al-doped ZnO Core-Shell Nanoparticles. *Sensors and Actuators, 10*, Article#31.

Yang, S. (2011). Novel Ga-doped, self-supported, independent aligned ZnO nanorods: one-pot hydrothermal synthesis and structurally enhanced photocatalytic performance. *RSC Advances, 1*, Article#4.

Yangyang. (2021). High Current Field Emission from Large-Area Indium Doped ZnO Nanowire Field Emitter Arrays for Flat-Panel X-ray Source Application. *Nanomaterials, 240*(11), Article#16.

Yi-Huang. (2019). Antibacterial Property of Composites of Reduced Graphene Oxide with Nano-Silver and Zinc Oxide Nanoparticles Synthesized Using a Microwave-Assisted Approach. *Molecular Sciences, 54*, Article#15.

Young, S.-J. (2016). Synthesis of Ga-Doped ZnO Nanorods by Hydrothermal Method and Their Application to Ultraviolet Photodetector. *inventions, 1*(1), Article#6.

Young, S. J. (2016). Synthesis and optoelectronic properties of Ga-doped ZnO nanorods by hydrothermal method. *Microsyst Technol, 6*, Article#5.

Yu-Hsuan. (2021). Rapid synthesis of microwave-assisted zinc oxide nanorods on a paper-based analytical device for fluorometric detection of L-dopa. *Colloids and Surfaces B: Biointerfaces, 207*, Article#6.

Zak, A. K. (2012). *Fabrication And Charavterization Of Zinc Oxide And Lead Zirconati Titanate Nanostructures.* (Doctor), University Of Malaya

Zhang, J. Z. (2009). Optical Properties Of Nanomaterials. *World Scientific, Singapore, 5*, Article#35.

Zhao, L., Deng, J., Sun, P., Liu, J., Ji, Y., Nakada, N., . . . Yang, Y. (2018). Nanomaterials for treating emerging contaminants in water by adsorption and photocatalysis: Systematic review and bibliometric analysis. *Sci Total Environ, 627*, Article#1253-1263.

Zhou, Q. (2017). Synthesis of Vertically-Aligned Zinc Oxide Nanowires and Their Application as a Photocatalyst. *nanomateryials, 7*(6), Article#13.